

UvA-DARE (Digital Academic Repository)

Determining the effects of clumping and porosity on the chemistry in a non-uniform AGB outflow

Van de Sande, M.; Sundqvist, J.O.; Millar, T.J.; Keller, D.; Homan, W.; de Koter, A.; Decin, L.; De Ceuster, F.

DOI

[10.1051/0004-6361/201732276](https://doi.org/10.1051/0004-6361/201732276)

Publication date

2018

Document Version

Other version

Published in

Astronomy & Astrophysics

[Link to publication](#)

Citation for published version (APA):

Van de Sande, M., Sundqvist, J. O., Millar, T. J., Keller, D., Homan, W., de Koter, A., Decin, L., & De Ceuster, F. (2018). Determining the effects of clumping and porosity on the chemistry in a non-uniform AGB outflow. *Astronomy & Astrophysics*, 616, [A106].
<https://doi.org/10.1051/0004-6361/201732276>

General rights

It is not permitted to download or to forward/distribute the text or part of it without the consent of the author(s) and/or copyright holder(s), other than for strictly personal, individual use, unless the work is under an open content license (like Creative Commons).

Disclaimer/Complaints regulations

If you believe that digital publication of certain material infringes any of your rights or (privacy) interests, please let the Library know, stating your reasons. In case of a legitimate complaint, the Library will make the material inaccessible and/or remove it from the website. Please Ask the Library: <https://uba.uva.nl/en/contact>, or a letter to: Library of the University of Amsterdam, Secretariat, Singel 425, 1012 WP Amsterdam, The Netherlands. You will be contacted as soon as possible.

UvA-DARE is a service provided by the library of the University of Amsterdam (<https://dare.uva.nl>)

Determining the effects of clumping and porosity on the chemistry in a non-uniform AGB outflow (Corrigendum)

M. Van de Sande¹, J. O. Sundqvist¹, T. J. Millar², D. Keller¹, W. Homan¹, A. de Koter^{3,1}, L. Decin^{1,4}, and F. De Ceuster⁵

¹ Department of Physics and Astronomy, Institute of Astronomy, KU Leuven, Celestijnenlaan 200D, 3001 Leuven, Belgium
e-mail: marie.vandesande@kuleuven.be

² Astrophysics Research Centre, School of Mathematics and Physics, Queen's University Belfast, University Road, Belfast BT7 1NN, UK

³ Astronomical Institute Anton Pannekoek, University of Amsterdam, Science Park 904, PO Box 94249, 1090 GE Amsterdam, The Netherlands

⁴ School of Chemistry, University of Leeds, Leeds LS2 9JT, UK

⁵ Department of Physics and Astronomy, University College London, Gower Street, London WC1E 6BT, UK

A&A, 616, A106 (2018), <https://doi.org/10.1051/0004-6361/201732276>

Key words. astrochemistry – molecular processes – circumstellar matter – stars: AGB and post-AGB – ISM: molecules – errata, addenda

When calculating the models discussed in the article, CO self-shielding was erroneously not taken into account. The CO photodissociation rates are therefore smaller than those used in the article. The lower photodissociation rate leads to a lower abundance of C and O close to the star, which influences our results. While clumping and porosity still affects the chemistry throughout the outflow, the formation of C-bearing species in O-rich outflows and vice versa is not as large, as their formation depends on the abundance of the deficient element. The chemistry of N- and S-bearing species is largely unaffected.

Figures 4 and 5 show the abundance profiles for the one- and two-component O-rich outflows. The corresponding column densities are listed in Tables 4 and 5, where changes larger than one order of magnitude are marked in boldface. While the abundance of NH₃ is largely unaffected, the peak fractional abundances of HCN and CS decrease from 10⁻⁷ to 10⁻¹⁰ relative to H₂, which does not correspond to observations of HCN and CS in O-rich outflows. The abundance of HCN and CS throughout the outflow are, however, still affected by clumping.

Figures 6 and 7 show the abundance profiles for the one- and two-component C-rich outflows. The corresponding column densities are listed in Tables 6 and 7. The NH₃ abundance profile is again largely unaffected. The peak fractional abundance of H₂O decreases from 10⁻⁵ to 10⁻⁸ relative to H₂, that of H₂S remains at ~10⁻⁸ relative to H₂. The maximum abundance of 10⁻⁸ relative to H₂ for H₂O corresponds to the lower end of the range of the H₂O abundance in C-rich outflows (Lombaert et al. 2016). Because of the lower C⁺ abundance, the abundance profiles of H₂O and H₂S do not show the secondary peak towards the end of the intermediate region.

The corrected abundance profiles of the additional molecules (Appendix E) for the one- and two-component O-rich outflows are shown in Figs. E.1 and E.2 for the O-rich outflows. The corresponding column densities are listed in Tables E.1 and E.2. The CH₄ abundance in the inner region increases up to an order of magnitude, in contrast to the previous increase of four orders

of magnitude, up to 10⁻⁶ relative to H₂. The overall H₂CO abundance has decreased, now reaching up to 10⁻¹¹ relative to H₂ with an increase of about an order of magnitude caused by clumping at the end of the intermediate wind. The increase in inner wind abundance of up to four orders of magnitude is not present. Similarly, the C₂H₂ and CN overall abundance has decreased by up to two orders of magnitude. The abundance of C₂H₂ does not increase relative to the smooth outflow in the inner wind, and therefore does not reach up to 10⁻⁸ relative to H₂ in this region, while the increase in CN abundance has decreased from 10⁻⁷ to 10⁻¹¹ relative to H₂. The behaviour of the parent species SO is largely unaffected.

Figures E.3 and E.4 show the corrected abundance profiles of the additional molecules for the one- and two-component C-rich outflows. The corresponding column densities are listed in Tables E.3 and E.4. The overall OH abundance decreases by up to two orders of magnitude. Clumping does not lead to a peak abundance in the inner wind of 10⁻⁷ relative to H₂, but still leads to an increase of up to an order of magnitude. The overall H₂CO abundance has decreased by up to two order of magnitude. Clumping leads to an increase in the inner wind abundance, although also two orders magnitude lower. The abundances of HC₃N, CH₃CN, and C₄H₂ are largely unaffected.

The corrected abundance profiles of Appendix F, on the predictability of the models, are shown in Figs. F.1 and F.2 for the O-rich outflows. The corresponding column densities are listed in Tables F.1 and F.2. Although the N₂O peak abundance has decreased by an order of magnitude, clumping still causes an increase of up to five orders of magnitude. The peak C₂N abundance has decreased by more than two orders of magnitude. While clumping causes an increase of up to an order of magnitude in the outer wind, the peak inner wind abundance drops from 10⁻⁹ to 10⁻¹⁶ relative to H₂. The abundance profiles of C₃H and C₃H₂ show a similar behaviour. The OCS abundance profile does not show a peak towards the end of the intermediate outflow. Clumping can cause an increase of up to an order of magnitude to ~10⁻¹⁰ relative to H₂ in the intermediate outflow,

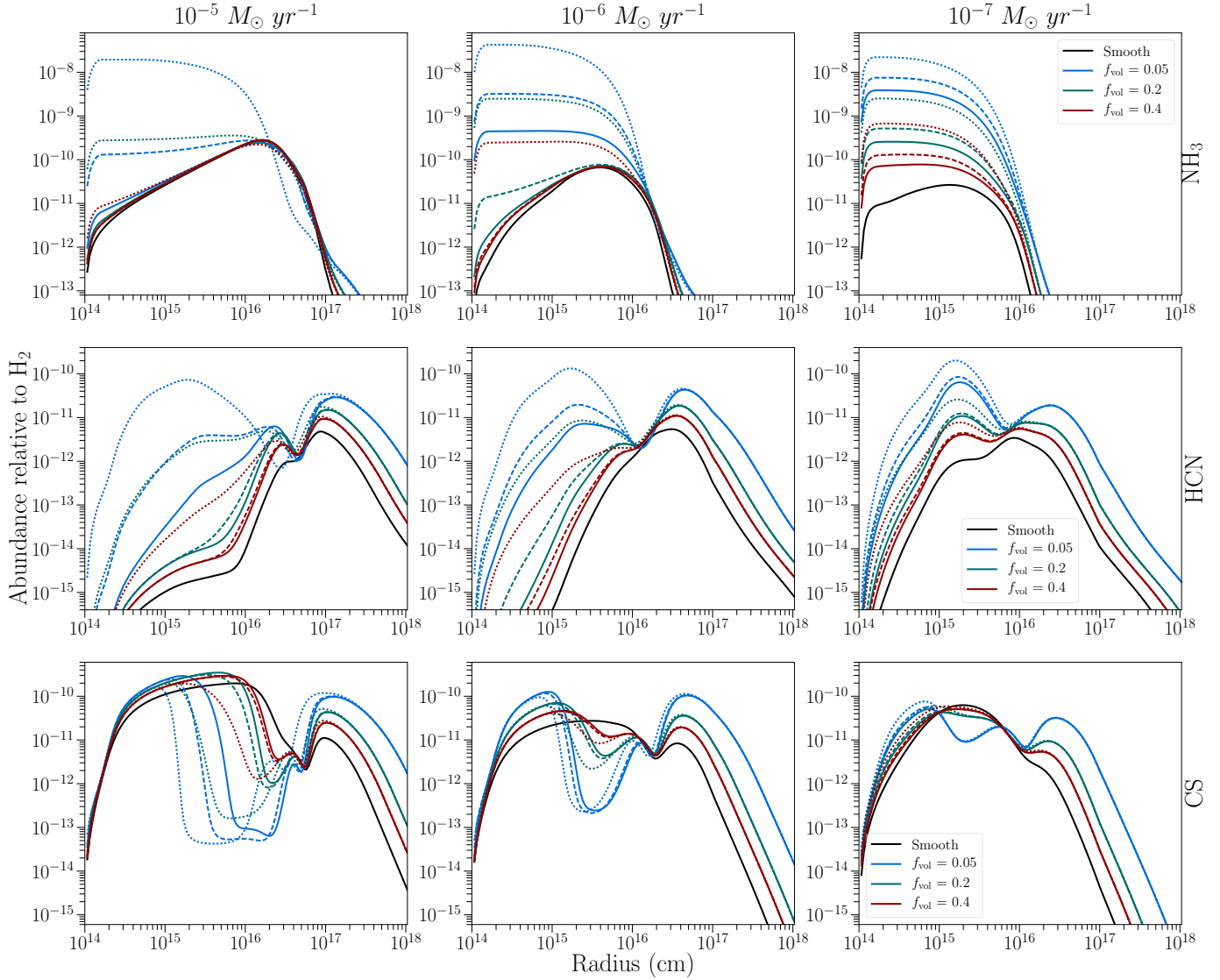


Fig. 4. Abundance of NH_3 (upper panels), HCN (middle panels), and CS (lower panels) relative to H_2 throughout a one-component O-rich outflow with different mass-loss rates \dot{M} and clump volume filling factors f_{vol} . Solid black line: calculated abundance for a smooth, uniform outflow. Solid coloured line: characteristic clump scale $l_* = 5 \times 10^{12} \text{ cm}$, porosity length $h_* = 1 \times 10^{14}, 2.5 \times 10^{13}, 1.25 \times 10^{13} \text{ cm}$ for $f_{\text{vol}} = 0.05, 0.2, 0.4$, respectively. Dashed coloured line: $l_* = 10^{13} \text{ cm}$, $h_* = 2 \times 10^{14}, 5 \times 10^{13}, 2.5 \times 10^{13} \text{ cm}$ for $f_{\text{vol}} = 0.05, 0.2, 0.4$, respectively. Dotted coloured line: $l_* = 5 \times 10^{13} \text{ cm}$, $h_* = 1 \times 10^{15}, 2.5 \times 10^{14}, 1.25 \times 10^{14} \text{ cm}$ for $f_{\text{vol}} = 0.05, 0.2, 0.4$, respectively. We note that models with $f_{\text{vol}} = 0.2$, $l_* = 5 \times 10^{12} \text{ cm}$ (green, solid) and $f_{\text{vol}} = 0.4$, $l_* = 1 \times 10^{13} \text{ cm}$ (red, dashed) have the same porosity length $h_* = 2.5 \times 10^{13} \text{ cm}$. For reference, $1 R_* = 5 \times 10^{13} \text{ cm}$.

in contrast to abundances up to 10^{-7} relative to H_2 in the inner wind.

Figures F.3 and F.4 show the corrected abundance profiles of Appendix F for the one- and two-component C-rich outflows. The corresponding column densities are listed in Tables F.3 and F.4. Clumping can cause an increase of up to four orders of magnitude in the inner wind CO_2 , although the peak abundance drops from 10^{-7} to 10^{-9} relative to H_2 . The SO_2 abundance is drastically affected: the peak abundance of the smooth outflow goes down by four orders of magnitude. Clumping can cause an increase of up to three orders of magnitude, although only up to 10^{-13} relative to H_2 in contrast with the previous 10^{-9} relative to H_2 . While the overall HC_9N abundance has decreased by more than an order of magnitude, clumping can still cause an increase in peak abundance of up to three orders of magnitude. The abundance profiles of NO and OCS show similar behaviour,

although clumping now increases the peak abundance only up to one to two orders of magnitude, respectively, in contrast with the previous increase of two to four orders of magnitude.

When comparing our results to those of Agúndez et al. (2010), the models still differ in shape, but our models now produce lower abundances of C-bearing species in O-rich outflows and vice versa than Agúndez et al. (2010). We note that our model differs from that of Agúndez et al. (2010) not only in implementation of the density distribution and alteration of the UV radiation field, but also in the chemical reaction network used. Our models still produce NH_3 with a larger abundance than TE , unlike non-equilibrium chemistry models.

References

- Agúndez, M., Cernicharo, J., & Guélin, M. 2010, *ApJ*, 724, L133
Lombaert, R., Decin, L., Royer, P., et al. 2016, *A&A*, 588, A124

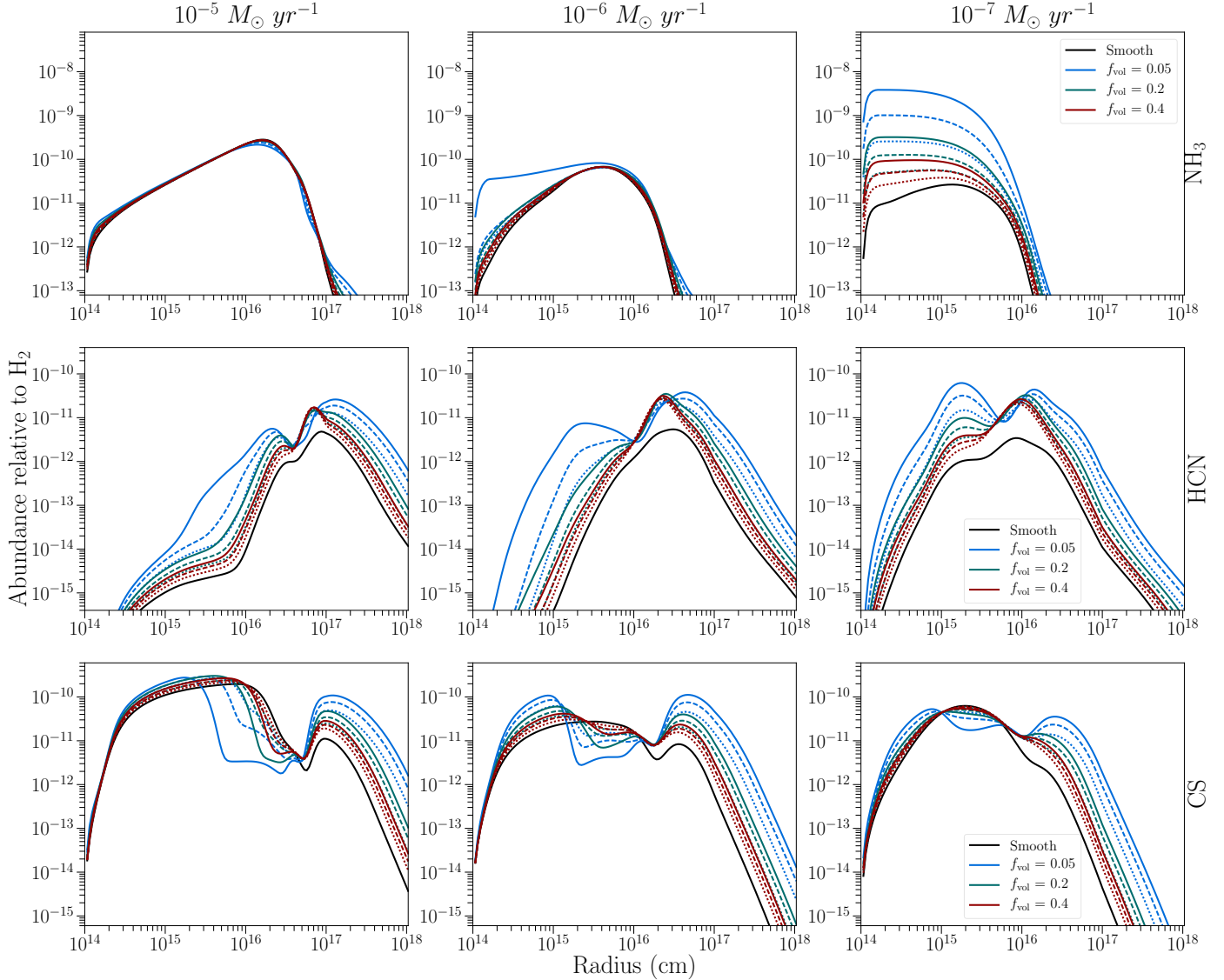


Fig. 5. Abundance of NH_3 (upper panels), HCN (middle panels), and CS (lower panels) relative to H_2 throughout a two-component O-rich outflow with different mass-loss rates \dot{M} and clump volume filling factors f_{vol} . The characteristic size of the clumps at the stellar radius is $l_* = 10^{13} \text{ cm}$. Blue lines: porosity length $h_* = 2 \times 10^{14} \text{ cm}$. Green lines: $h_* = 5 \times 10^{13} \text{ cm}$. Red lines: $h_* = 2.5 \times 10^{13} \text{ cm}$. Solid black line: calculated abundance for a smooth, uniform outflow. Solid coloured line: density contrast between the inter-clump and smooth outflow $f_{\text{ic}} = 0.1$. Dashed coloured line: $f_{\text{ic}} = 0.3$. Dotted coloured line: $f_{\text{ic}} = 0.5$. We note that the models with $f_{\text{vol}} = 0.4$ (red) have the same porosity length as the one-component outflows with $f_{\text{vol}} = 0.2$, $l_* 5 \times 10^{12} \text{ cm}$ and $f_{\text{vol}} = 0.4$, $l_* = 1 \times 10^{13} \text{ cm}$. For reference, $1 R_* = 5 \times 10^{13} \text{ cm}$.

Table 4. Column density [cm^{-2}] of NH_3 , HCN, and CS in a smooth O-rich outflow with different mass-loss rates, together with column density ratios relative to the smooth outflow for specific one-component outflows.

| \dot{M} $10^{-5} M_{\odot} \text{yr}^{-1}$ | Species | NH ₃ | | | HCN | | | CS | | | |
|---|-------------------------------------|------------------|---------|--------------------------------------|--------------------------------------|----------------|-----------------------------------|-----------------------------------|----------------|---------------------------------|------|
| | | Smooth | | | $9.1 \times 10^{11} \text{ cm}^{-2}$ | | | $5.9 \times 10^8 \text{ cm}^{-2}$ | | | |
| | | f_{vol} | 0.05 | 0.2 | 0.4 | 0.05 | 0.2 | 0.4 | 0.05 | 0.2 | |
| $l_* = 5 \times 10^{12} \text{ cm}$ | Smooth | 1.3e+00 | 1.1e+00 | 1.1e+00 | 9.8e+00 | 3.7e+00 | 2.1e+00 | 1.7e+00 | 1.7e+00 | 1.5e+00 | |
| | $f_{\text{vol}} = 0.2$ | 9.6e+00 | 1.1e+00 | 1.1e+00 | 4.5e+01 | 4.1e+00 | 2.2e+00 | 1.5e+00 | 1.7e+00 | 1.5e+00 | |
| | $f_{\text{vol}} = 0.4$ | 1.3e+03 | 2.0e+01 | 1.4e+00 | 1.3e+03 | 3.8e+01 | 4.2e+00 | 1.0e+00 | 1.2e+00 | 1.2e+00 | |
| $10^{-6} M_{\odot} \text{yr}^{-1}$ | Smooth | | | $4.6 \times 10^{10} \text{ cm}^{-2}$ | | | $2.8 \times 10^8 \text{ cm}^{-2}$ | | | 4.6e+10 cm^{-2} | |
| | f_{vol} | 0.05 | 0.2 | 0.4 | 0.05 | 0.2 | 0.4 | 0.05 | 0.2 | 0.4 | 0.05 |
| | $l_* = 5 \times 10^{12} \text{ cm}$ | 6.1e+01 | 1.4e+00 | 1.2e+00 | 1.8e+01 | 3.1e+00 | 1.9e+00 | 4.1e+00 | 2.5e+00 | 1.7e+00 | |
| $l_* = 1 \times 10^{13} \text{ cm}$ | Smooth | 4.3e+02 | 3.1e+00 | 1.3e+00 | 5.5e+01 | 3.6e+00 | 2.0e+00 | 3.9e+00 | 2.4e+00 | 1.7e+00 | |
| | $f_{\text{vol}} = 0.2$ | 5.6e+03 | 3.3e+02 | 3.4e+01 | 4.3e+02 | 2.4e+01 | 4.2e+00 | 3.3e+00 | 2.1e+00 | 1.6e+00 | |
| | $f_{\text{vol}} = 0.4$ | | | | | | | | | | |
| $10^{-7} M_{\odot} \text{yr}^{-1}$ | Smooth | | | $8.1 \times 10^9 \text{ cm}^{-2}$ | | | $1.0 \times 10^8 \text{ cm}^{-2}$ | | | 6.0e+09 cm^{-2} | |
| | f_{vol} | 0.05 | 0.2 | 0.4 | 0.05 | 0.2 | 0.4 | 0.05 | 0.2 | 0.4 | 0.05 |
| | $l_* = 5 \times 10^{12} \text{ cm}$ | 2.8e+02 | 1.8e+01 | 5.3e+00 | 3.5e+01 | 6.4e+00 | 2.8e+00 | 1.4e+00 | 1.1e+00 | 1.0e+00 | |
| $l_* = 1 \times 10^{13} \text{ cm}$ | Smooth | 5.4e+02 | 3.7e+01 | 9.3e+00 | 5.0e+01 | 7.6e+00 | 3.1e+00 | 1.6e+00 | 1.2e+00 | 1.1e+00 | |
| | $f_{\text{vol}} = 0.2$ | 1.6e+03 | 1.8e+02 | 4.7e+01 | 1.4e+02 | 1.9e+01 | 6.0e+00 | 2.2e+00 | 1.8e+00 | 1.5e+00 | |
| | $f_{\text{vol}} = 0.4$ | | | | | | | | | | |

Notes. The corresponding abundance profiles are shown in Fig. 4. We note that the models with $f_{\text{vol}} = 0.2$, $l_* = 5 \times 10^{12} \text{ cm}$ and $f_{\text{vol}} = 0.4$, $l_* = 1 \times 10^{13} \text{ cm}$ have the same porosity length $h_* = 2.5 \times 10^{13} \text{ cm}$. Changes larger than one order of magnitude are in boldface.

Table 5. Column density [cm^{-2}] of NH₃, HCN, and CS in a smooth O-rich outflow with different mass-loss rates, together with column density ratios relative to the smooth outflow for specific two-component outflows.

| \dot{M} $10^{-5} M_{\odot} \text{yr}^{-1}$ | Species | NH ₃ | | | HCN | | | CS | | | |
|---|------------------------|------------------|---------|--------------------------------------|--------------------------------------|---------|-----------------------------------|-----------------------------------|---------|---------------------------------|------|
| | | Smooth | | | $9.1 \times 10^{11} \text{ cm}^{-2}$ | | | $5.9 \times 10^8 \text{ cm}^{-2}$ | | | |
| | | f_{vol} | 0.05 | 0.2 | 0.4 | 0.05 | 0.2 | 0.4 | 0.05 | 0.2 | |
| $f_{\text{ic}} = 0.1$ | Smooth | 1.1e+00 | 1.1e+00 | 1.1e+00 | 8.7e+00 | 4.3e+00 | 3.2e+00 | 1.6e+00 | 1.6e+00 | 1.4e+00 | |
| | $f_{\text{vol}} = 0.2$ | 1.1e+00 | 1.1e+00 | 1.1e+00 | 5.8e+00 | 3.5e+00 | 3.0e+00 | 1.5e+00 | 1.4e+00 | 1.3e+00 | |
| | $f_{\text{vol}} = 0.4$ | 1.1e+00 | 1.1e+00 | 1.2e+00 | 4.3e+00 | 3.1e+00 | 3.0e+00 | 1.4e+00 | 1.3e+00 | 1.2e+00 | |
| $10^{-6} M_{\odot} \text{yr}^{-1}$ | Smooth | | | $4.6 \times 10^{10} \text{ cm}^{-2}$ | | | $2.8 \times 10^8 \text{ cm}^{-2}$ | | | 4.6e+10 cm^{-2} | |
| | f_{vol} | 0.05 | 0.2 | 0.4 | 0.05 | 0.2 | 0.4 | 0.05 | 0.2 | 0.4 | 0.05 |
| | $f_{\text{ic}} = 0.1$ | 5.7e+00 | 1.3e+00 | 1.2e+00 | 1.8e+01 | 4.9e+00 | 3.9e+00 | 3.6e+00 | 2.2e+00 | 1.6e+00 | |
| $f_{\text{ic}} = 0.3$ | Smooth | 1.4e+00 | 1.2e+00 | 1.2e+00 | 7.0e+00 | 4.2e+00 | 3.8e+00 | 2.9e+00 | 1.8e+00 | 1.4e+00 | |
| | $f_{\text{vol}} = 0.2$ | 1.2e+00 | 1.2e+00 | 1.2e+00 | 4.7e+00 | 3.9e+00 | 3.8e+00 | 2.2e+00 | 1.5e+00 | 1.3e+00 | |
| | $f_{\text{vol}} = 0.4$ | | | | | | | | | | |
| $10^{-7} M_{\odot} \text{yr}^{-1}$ | Smooth | | | $8.1 \times 10^9 \text{ cm}^{-2}$ | | | $1.0 \times 10^8 \text{ cm}^{-2}$ | | | 6.0e+09 cm^{-2} | |
| | f_{vol} | 0.05 | 0.2 | 0.4 | 0.05 | 0.2 | 0.4 | 0.05 | 0.2 | 0.4 | 0.05 |
| | $f_{\text{ic}} = 0.1$ | 2.8e+02 | 2.3e+01 | 6.7e+00 | 3.6e+01 | 7.9e+00 | 4.6e+00 | 1.5e+00 | 1.2e+00 | 1.1e+00 | |
| $f_{\text{ic}} = 0.3$ | Smooth | 7.3e+01 | 9.0e+00 | 3.7e+00 | 1.9e+01 | 5.6e+00 | 3.9e+00 | 1.3e+00 | 1.2e+00 | 1.2e+00 | |
| | $f_{\text{vol}} = 0.2$ | 1.8e+01 | 3.8e+00 | 2.3e+00 | 9.6e+00 | 4.2e+00 | 3.6e+00 | 1.2e+00 | 1.2e+00 | 1.3e+00 | |
| | $f_{\text{vol}} = 0.4$ | | | | | | | | | | |

Notes. The corresponding abundance profiles are shown in Fig. 5. We note that models with $f_{\text{vol}} = 0.4$ have the same porosity length $h_* = 2.5 \times 10^{13} \text{ cm}$ as the one-component models with $f_{\text{vol}} = 0.2$, $l_* = 5 \times 10^{12} \text{ cm}$ and $f_{\text{vol}} = 0.4$, $l_* = 1 \times 10^{13} \text{ cm}$. Changes larger than one order of magnitude are in boldface.

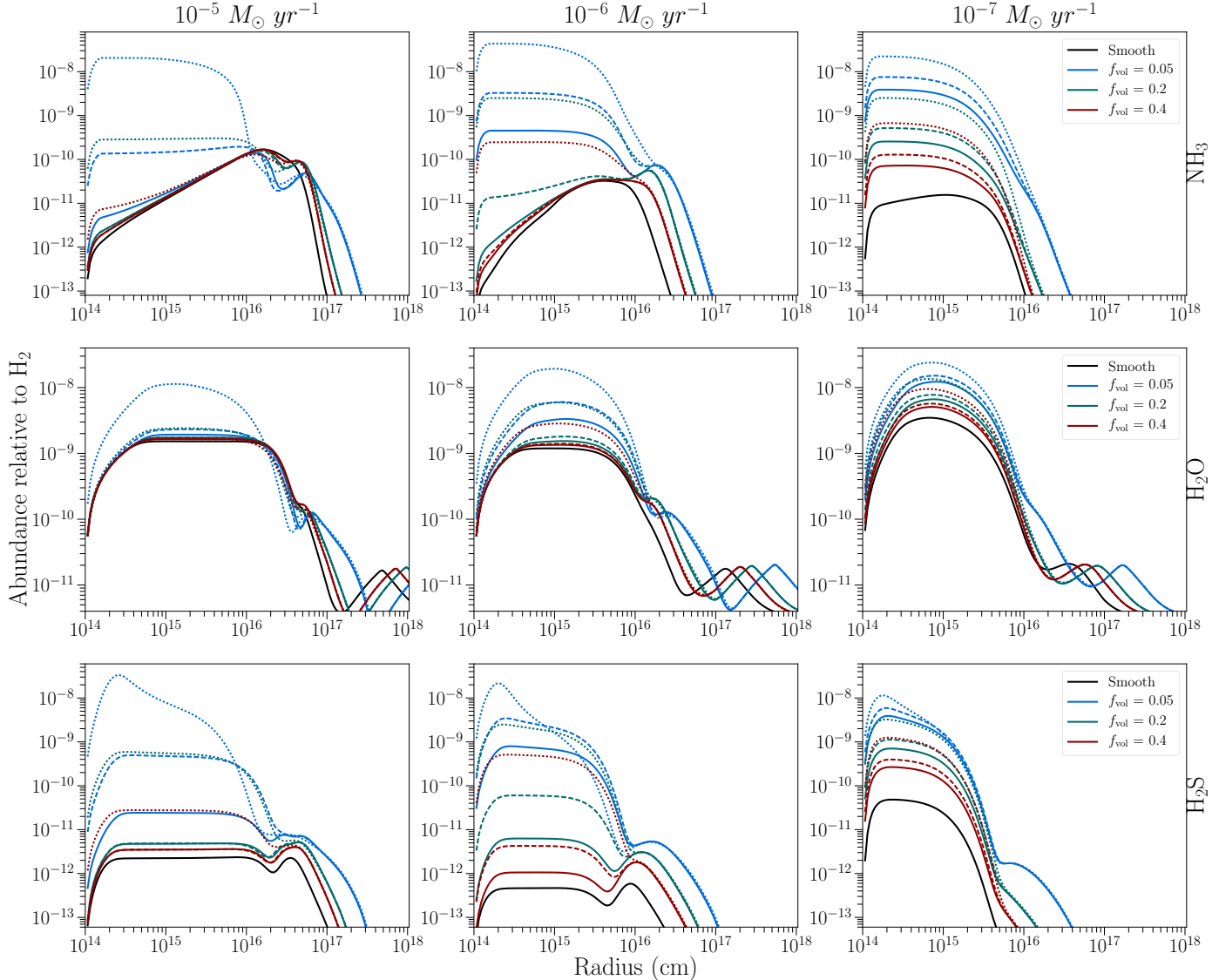


Fig. 6. Abundance of NH_3 (upper panels), H_2O (middle panels), and H_2S (lower panels) relative to H_2 throughout a one-component C-rich outflow with different mass-loss rates \dot{M} and clump volume filling factors f_{vol} . Solid black line: calculated abundance for a smooth, uniform outflow. Solid coloured line: characteristic clump scale $l_* = 5 \times 10^{12} \text{ cm}$, porosity length $h_* = 1 \times 10^{14}, 2.5 \times 10^{13}, 1.25 \times 10^{13} \text{ cm}$ for $f_{\text{vol}} = 0.05, 0.2, 0.4$, respectively. Dashed coloured line: $l_* = 10^{13} \text{ cm}$, $h_* = 2 \times 10^{14}, 5 \times 10^{13}, 2.5 \times 10^{13} \text{ cm}$ for $f_{\text{vol}} = 0.05, 0.2, 0.4$, respectively. Dotted coloured line: $l_* = 5 \times 10^{13} \text{ cm}$, $h_* = 1 \times 10^{15}, 2.5 \times 10^{14}, 1.25 \times 10^{14} \text{ cm}$ for $f_{\text{vol}} = 0.05, 0.2, 0.4$, respectively. We note that models with $f_{\text{vol}} = 0.2$, $l_* = 5 \times 10^{12} \text{ cm}$ (green, solid) and $f_{\text{vol}} = 0.4$, $l_* = 1 \times 10^{13} \text{ cm}$ (red, dashed) have the same porosity length $h_* = 2.5 \times 10^{13} \text{ cm}$. For reference, $1 R_* = 5 \times 10^{13} \text{ cm}$.

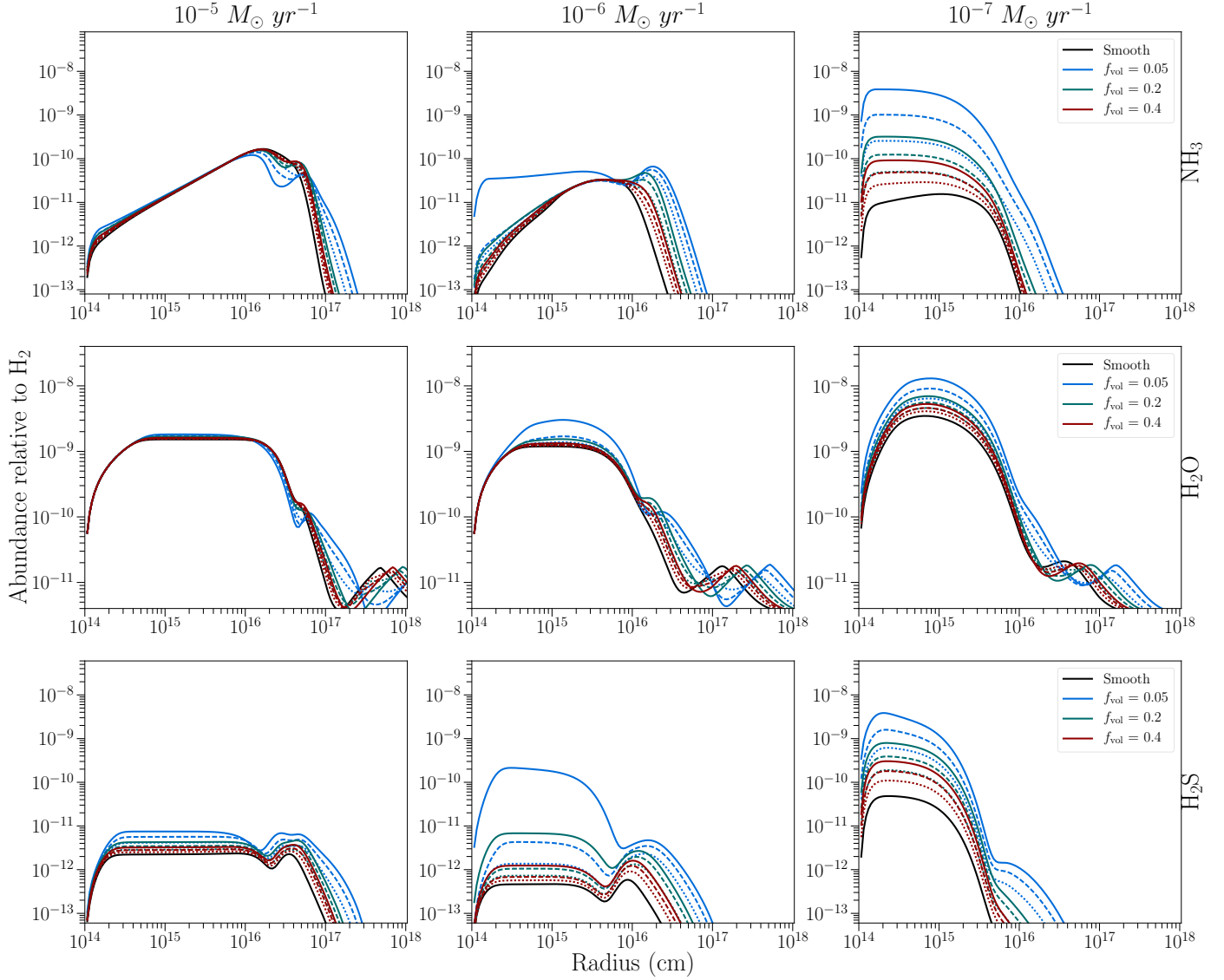


Fig. 7. Abundance of NH_3 (upper panels), H_2O (middle panels), and H_2S (lower panels) relative to H_2 throughout a two-component C-rich outflow with different mass-loss rates \dot{M} and clump volume filling factors f_{vol} . The characteristic size of the clumps at the stellar radius is $l_* = 10^{13} \text{ cm}$. Blue lines: porosity length $h_* = 2 \times 10^{14} \text{ cm}$. Green lines: $h_* = 5 \times 10^{13} \text{ cm}$. Red lines: $h_* = 2.5 \times 10^{13} \text{ cm}$. Solid black line: calculated abundance for a smooth, uniform outflow. Solid coloured line: density contrast between the inter-clump and smooth outflow $f_{\text{ic}} = 0.1$. Dashed coloured line: $f_{\text{ic}} = 0.3$. Dotted coloured line: $f_{\text{ic}} = 0.5$. We note that the models with $f_{\text{vol}} = 0.4$ (red) have the same porosity length as the one-component outflows with $f_{\text{vol}} = 0.2$, $l_* = 5 \times 10^{12} \text{ cm}$ and $f_{\text{vol}} = 0.4$, $l_* = 1 \times 10^{13} \text{ cm}$. For reference, $1 R_* = 5 \times 10^{13} \text{ cm}$.

Table 6. Column density [cm^{-2}] of NH_3 , H_2O , and H_2S in a smooth C-rich outflow with different mass-loss rates, together with column density ratios relative to the smooth outflow for specific one-component outflows.

| \dot{M} $10^{-5} M_{\odot} \text{yr}^{-1}$ | Species | NH_3 | | | H_2O | | | H_2S | | |
|---|------------------------|------------------|------------------|---------|--------------------------------------|----------------|------------------|--------------------------------------|---------|------------------|
| | | Smooth | | | $4.8 \times 10^{11} \text{ cm}^{-2}$ | | | $5.5 \times 10^{13} \text{ cm}^{-2}$ | | |
| | | f_{vol} | 0.05 | 0.2 | 0.4 | 0.05 | 0.2 | 0.4 | 0.05 | 0.2 |
| $l_* = 5 \times 10^{12} \text{ cm}$ | Smooth | 1.4e+00 | 1.2e+00 | 1.1e+00 | 1.1e+00 | 1.1e+00 | 1.0e+00 | 9.1e+00 | 2.0e+00 | 1.5e+00 |
| | $f_{\text{vol}} = 0.2$ | 1.8e+01 | 1.1e+00 | 1.1e+00 | 1.3e+00 | 1.1e+00 | 1.0e+00 | 1.8e+02 | 2.0e+00 | 1.5e+00 |
| | $f_{\text{vol}} = 0.4$ | 2.6e+03 | 3.8e+01 | 1.8e+00 | 5.1e+00 | 1.3e+00 | 1.1e+00 | 9.1e+03 | 2.4e+02 | 1.2e+01 |
| $l_* = 1 \times 10^{13} \text{ cm}$ | Smooth | 2.3e+10 | cm^{-2} | | | 4.7e+12 | cm^{-2} | | 2.5e+09 | cm^{-2} |
| | f_{vol} | 0.05 | 0.2 | 0.4 | 0.05 | 0.2 | 0.4 | 0.05 | 0.2 | 0.4 |
| | $f_{\text{vol}} = 0.2$ | 1.2e+02 | 1.6e+00 | 1.3e+00 | 1.9e+00 | 1.1e+00 | 1.1e+00 | 1.4e+03 | 1.2e+01 | 2.1e+00 |
| $l_* = 5 \times 10^{13} \text{ cm}$ | Smooth | 8.9e+02 | 4.9e+00 | 1.3e+00 | 3.3e+00 | 1.2e+00 | 1.1e+00 | 5.7e+03 | 1.2e+02 | 8.4e+00 |
| | $f_{\text{vol}} = 0.2$ | 1.2e+04 | 6.8e+02 | 6.9e+01 | 1.1e+01 | 3.7e+00 | 1.9e+00 | 2.7e+04 | 4.7e+03 | 1.0e+03 |
| | $f_{\text{vol}} = 0.4$ | | | | | | | | | |
| $l_* = 5 \times 10^{12} \text{ cm}$ | Smooth | 6.5e+09 | cm^{-2} | | | 1.1e+12 | cm^{-2} | | 2.3e+10 | cm^{-2} |
| | f_{vol} | 0.05 | 0.2 | 0.4 | 0.05 | 0.2 | 0.4 | 0.05 | 0.2 | 0.4 |
| | $f_{\text{vol}} = 0.2$ | 3.5e+02 | 2.3e+01 | 6.3e+00 | 3.1e+00 | 1.8e+00 | 1.4e+00 | 7.4e+01 | 1.4e+01 | 5.5e+00 |
| $l_* = 1 \times 10^{13} \text{ cm}$ | Smooth | 6.7e+02 | 4.6e+01 | 1.1e+01 | 4.1e+00 | 2.1e+00 | 1.6e+00 | 1.1e+02 | 2.3e+01 | 8.3e+00 |
| | $f_{\text{vol}} = 0.2$ | 2.0e+03 | 2.2e+02 | 5.8e+01 | 6.8e+00 | 4.0e+00 | 2.9e+00 | 1.9e+02 | 6.6e+01 | 2.6e+01 |
| | $f_{\text{vol}} = 0.4$ | | | | | | | | | |

Notes. The corresponding abundance profiles are shown in Fig. 6. We note that the models with $f_{\text{vol}} = 0.2$, $l_* = 5 \times 10^{12} \text{ cm}$ and $f_{\text{vol}} = 0.4$, $l_* = 1 \times 10^{13} \text{ cm}$ have the same porosity length $h_* = 2.5 \times 10^{13} \text{ cm}$. Changes larger than one order of magnitude are in boldface.

Table 7. Column density [cm^{-2}] of NH_3 , H_2O , and H_2S in a smooth C-rich outflow with different mass-loss rates, together with column density ratios relative to the smooth outflow for specific two-component outflows.

| \dot{M} $10^{-5} M_{\odot} \text{yr}^{-1}$ | Species | NH_3 | | | H_2O | | | H_2S | | |
|---|------------------------|------------------|------------------|---------|--------------------------------------|------------------|---------|--------------------------------------|------------------|---------|
| | | Smooth | | | $4.8 \times 10^{11} \text{ cm}^{-2}$ | | | $5.5 \times 10^{13} \text{ cm}^{-2}$ | | |
| | | f_{vol} | 0.05 | 0.2 | 0.4 | 0.05 | 0.2 | 0.4 | 0.05 | 0.2 |
| $f_{\text{ic}} = 0.1$ | Smooth | 1.1e+00 | 1.1e+00 | 1.1e+00 | 1.1e+00 | 1.1e+00 | 1.1e+00 | 2.9e+00 | 1.8e+00 | 1.4e+00 |
| | $f_{\text{vol}} = 0.2$ | 1.1e+00 | 1.1e+00 | 1.1e+00 | 1.1e+00 | 1.1e+00 | 1.1e+00 | 2.2e+00 | 1.5e+00 | 1.3e+00 |
| | $f_{\text{vol}} = 0.4$ | 1.1e+00 | 1.1e+00 | 1.2e+00 | 1.1e+00 | 1.1e+00 | 1.2e+00 | 1.7e+00 | 1.3e+00 | 1.2e+00 |
| $f_{\text{ic}} = 0.1$ | Smooth | 2.3e+10 | cm^{-2} | | 4.7e+12 | cm^{-2} | | 2.5e+09 | cm^{-2} | |
| | f_{vol} | 0.05 | 0.2 | 0.4 | 0.05 | 0.2 | 0.4 | 0.05 | 0.2 | 0.4 |
| | $f_{\text{vol}} = 0.2$ | 1.0e+01 | 1.4e+00 | 1.2e+00 | 1.7e+00 | 1.1e+00 | 1.1e+00 | 3.4e+02 | 1.2e+01 | 2.4e+00 |
| $f_{\text{ic}} = 0.3$ | Smooth | 1.5e+00 | 1.3e+00 | 1.2e+00 | 1.2e+00 | 1.1e+00 | 1.1e+00 | 6.9e+00 | 2.1e+00 | 1.5e+00 |
| | $f_{\text{vol}} = 0.2$ | 1.3e+00 | 1.2e+00 | 1.2e+00 | 1.1e+00 | 1.1e+00 | 1.2e+00 | 2.6e+00 | 1.6e+00 | 1.3e+00 |
| | $f_{\text{vol}} = 0.4$ | | | | | | | | | |
| $f_{\text{ic}} = 0.1$ | Smooth | 6.5e+09 | cm^{-2} | | 1.1e+12 | cm^{-2} | | 2.3e+10 | cm^{-2} | |
| | f_{vol} | 0.05 | 0.2 | 0.4 | 0.05 | 0.2 | 0.4 | 0.05 | 0.2 | 0.4 |
| | $f_{\text{vol}} = 0.2$ | 3.4e+02 | 2.8e+01 | 8.0e+00 | 3.5e+00 | 2.0e+00 | 1.5e+00 | 7.3e+01 | 1.6e+01 | 6.3e+00 |
| $f_{\text{ic}} = 0.3$ | Smooth | 9.0e+01 | 1.1e+01 | 4.3e+00 | 2.5e+00 | 1.6e+00 | 1.4e+00 | 3.1e+01 | 8.1e+00 | 3.8e+00 |
| | $f_{\text{vol}} = 0.2$ | 2.3e+01 | 4.5e+00 | 2.5e+00 | 1.8e+00 | 1.4e+00 | 1.4e+00 | 1.2e+01 | 4.0e+00 | 2.4e+00 |
| | $f_{\text{vol}} = 0.4$ | | | | | | | | | |

Notes. The corresponding abundance profiles are shown in Fig. 7. We note that models with $f_{\text{vol}} = 0.4$ have the same porosity length $h_* = 2.5 \times 10^{13} \text{ cm}$ as the one-component models with $f_{\text{vol}} = 0.2$, $l_* = 5 \times 10^{12} \text{ cm}$ and $f_{\text{vol}} = 0.4$, $l_* = 1 \times 10^{13} \text{ cm}$. Changes larger than one order of magnitude are in boldface.

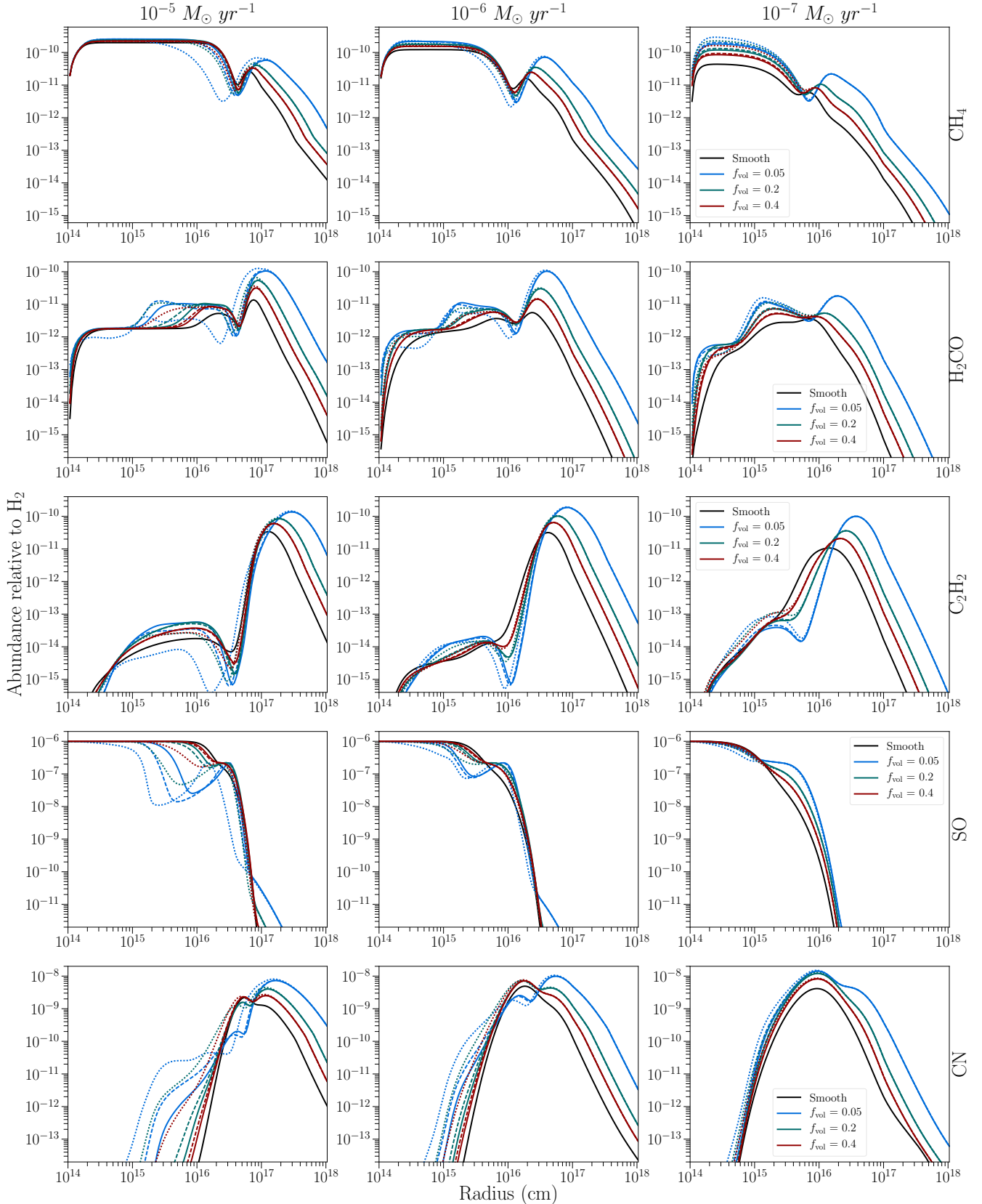


Fig. E.1. Abundance of CH_4 , H_2CO , C_2H_2 , SO and CN relative to H_2 throughout one-component O-rich outflow with different mass-loss rates M and clump volume filling factors f_{vol} . Solid black line: calculated abundance for a smooth, uniform outflow. Solid coloured line: characteristic clump scale $l_* = 5 \times 10^{12} \text{ cm}$, porosity length $h_* = 1 \times 10^{14}, 2.5 \times 10^{13}, 1.25 \times 10^{13} \text{ cm}$ for $f_{\text{vol}} = 0.05, 0.2, 0.4$, respectively. Dashed coloured line: $l_* = 10^{13} \text{ cm}$, $h_* = 2 \times 10^{14}, 5 \times 10^{13}, 2.5 \times 10^{13} \text{ cm}$ for $f_{\text{vol}} = 0.05, 0.2, 0.4$, respectively. Dotted coloured line: $l_* = 5 \times 10^{13} \text{ cm}$, $h_* = 1 \times 10^{15}, 2.5 \times 10^{14}, 1.25 \times 10^{14} \text{ cm}$ for $f_{\text{vol}} = 0.05, 0.2, 0.4$, respectively. We note that models with $f_{\text{vol}} = 0.2$, $l_* = 5 \times 10^{12} \text{ cm}$ (green, solid) and $f_{\text{vol}} = 0.4$, $l_* = 1 \times 10^{13} \text{ cm}$ (red, dashed) have the same porosity length $h_* = 2.5 \times 10^{13} \text{ cm}$. For reference, $1 R_* = 5 \times 10^{13} \text{ cm}$.

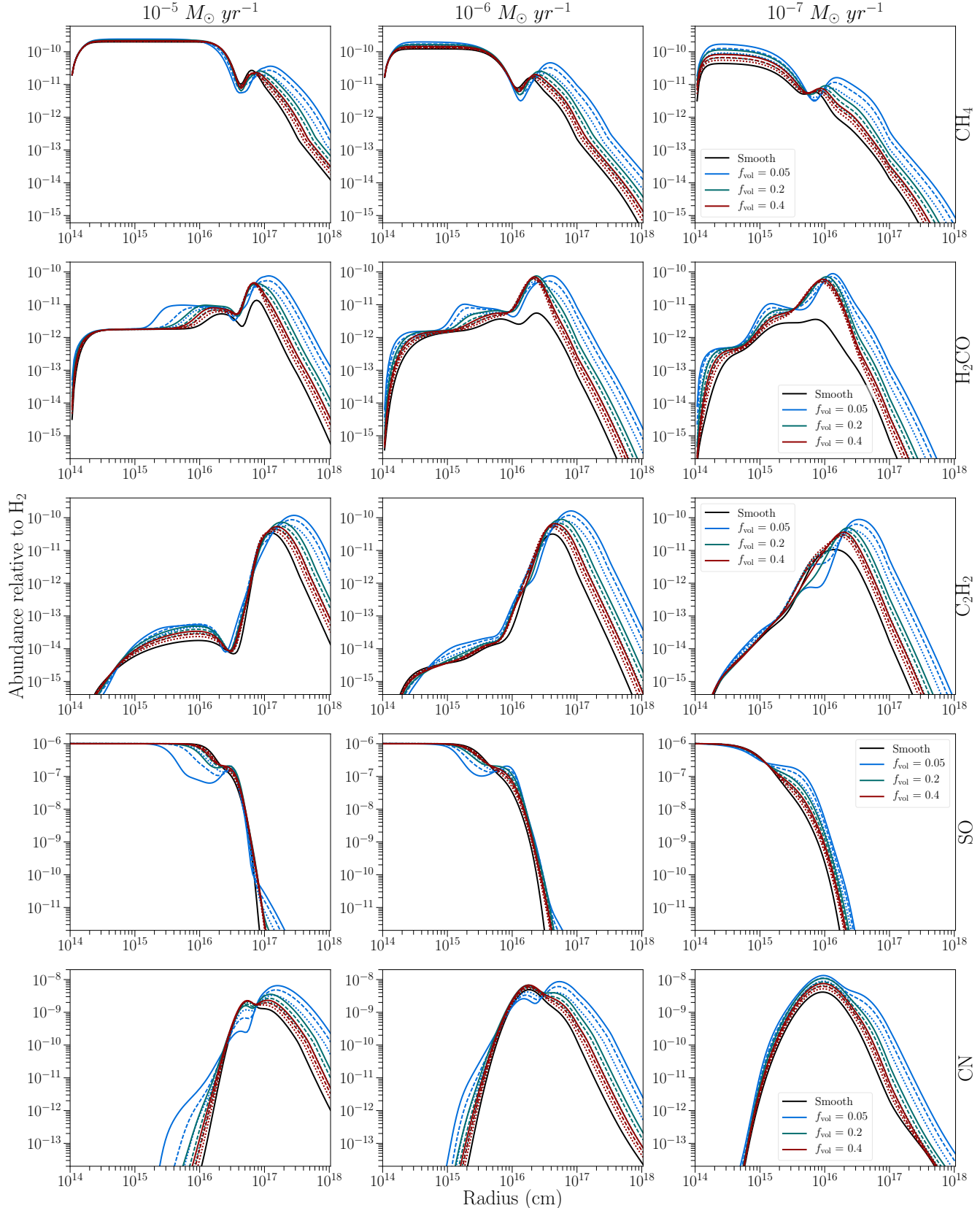


Fig. E.2. Abundance of CH_4 , H_2CO , C_2H_2 , SO , and CN relative to H_2 throughout a two-component O-rich outflow with different mass-loss rates \dot{M} and clump volume filling factors f_{vol} . The characteristic size of the clumps at the stellar radius is $l_* = 10^{13} \text{ cm}$. Blue lines: porosity length $h_* = 2 \times 10^{14} \text{ cm}$. Green lines: $h_* = 5 \times 10^{13} \text{ cm}$. Red lines: $h_* = 2.5 \times 10^{13} \text{ cm}$. Solid black line: calculated abundance for a smooth, uniform outflow. Solid coloured line: density contrast between the inter-clump and smooth outflow $f_{\text{ic}} = 0.1$. Dashed coloured line: $f_{\text{ic}} = 0.3$. Dotted coloured line: $f_{\text{ic}} = 0.5$. We note that the models with $f_{\text{vol}} = 0.4$ (red) have the same porosity length as the one-component outflows with $f_{\text{vol}} = 0.2$, $l_* = 5 \times 10^{12} \text{ cm}$ and $f_{\text{vol}} = 0.4$, $l_* = 1 \times 10^{13} \text{ cm}$. For reference, $1 R_* = 5 \times 10^{13} \text{ cm}$.

Table E.1. Column density [cm^{-2}] of CH_4 , H_2CO , C_2H_2 , SO , and CN in a smooth O-rich outflow with different mass-loss rates, together with column density ratios relative to the smooth outflow for specific one-component outflows.

| \dot{M} | Species | CH_4 | H_2CO | C_2H_2 | SO | CN |
|---|----------------|----------------------------------|----------------------------------|----------------------------------|----------------------------------|----------------------------------|
| $10^{-6} \text{ M}_{\odot} \text{ yr}^{-1}$ | Smooth | $1.1\text{e+13} \text{ cm}^{-2}$ | $7.5\text{e+10} \text{ cm}^{-2}$ | $1.8\text{e+09} \text{ cm}^{-2}$ | $7.5\text{e+16} \text{ cm}^{-2}$ | $2.8\text{e+11} \text{ cm}^{-2}$ |
| f_{vol} | 0.05 | 0.2 | 0.4 | 0.05 | 0.2 | 0.4 |
| $l_* = 5 \times 10^{12} \text{ cm}$ | 1.2e+00 | 1.1e+00 | 1.1e+00 | 1.7e+00 | 1.3e+00 | 0.05 |
| $l_* = 1 \times 10^{13} \text{ cm}$ | 1.2e+00 | 1.1e+00 | 1.1e+00 | 1.8e+00 | 1.2e+00 | 1.4e+00 |
| $l_* = 5 \times 10^{13} \text{ cm}$ | 1.2e+00 | 1.1e+00 | 1.1e+00 | 1.7e+00 | 1.3e+00 | 1.7e+00 |
| $10^{-5} \text{ M}_{\odot} \text{ yr}^{-1}$ | Smooth | $6.8\text{e+11} \text{ cm}^{-2}$ | $3.9\text{e+09} \text{ cm}^{-2}$ | $5.4\text{e+08} \text{ cm}^{-2}$ | $7.3\text{e+15} \text{ cm}^{-2}$ | $2.4\text{e+11} \text{ cm}^{-2}$ |
| f_{vol} | 0.05 | 0.2 | 0.4 | 0.05 | 0.2 | 0.4 |
| $l_* = 5 \times 10^{12} \text{ cm}$ | 1.6e+00 | 1.4e+00 | 1.2e+00 | 3.5e+00 | 2.2e+00 | 1.6e+00 |
| $l_* = 1 \times 10^{13} \text{ cm}$ | 1.6e+00 | 1.4e+00 | 1.2e+00 | 3.3e+00 | 2.3e+00 | 1.6e+00 |
| $l_* = 5 \times 10^{13} \text{ cm}$ | 1.6e+00 | 1.4e+00 | 1.3e+00 | 2.3e+00 | 2.4e+00 | 2.0e+00 |
| $10^{-4} \text{ M}_{\odot} \text{ yr}^{-1}$ | Smooth | $2.3\text{e+10} \text{ cm}^{-2}$ | $2.5\text{e+08} \text{ cm}^{-2}$ | $9.1\text{e+07} \text{ cm}^{-2}$ | $6.4\text{e+14} \text{ cm}^{-2}$ | $5.5\text{e+10} \text{ cm}^{-2}$ |
| f_{vol} | 0.05 | 0.2 | 0.4 | 0.05 | 0.2 | 0.4 |
| $l_* = 5 \times 10^{12} \text{ cm}$ | 3.9e+00 | 2.7e+00 | 1.9e+00 | 4.0e+00 | 2.6e+00 | 1.1e+00 |
| $l_* = 1 \times 10^{13} \text{ cm}$ | 4.3e+00 | 3.0e+00 | 2.1e+00 | 4.1e+00 | 2.6e+00 | 1.3e+00 |
| $l_* = 5 \times 10^{13} \text{ cm}$ | 6.1e+00 | 5.0e+00 | 3.7e+00 | 5.0e+00 | 4.3e+00 | 2.3e+00 |

Table E.2. Column density [cm^{-2}] of CH_4 , H_2CO , C_2H_2 , SO , and CN in a smooth O-rich outflow with different mass-loss rates, together with column density ratios relative to the smooth outflow for specific two-component outflows.

| \dot{M} | Species | CH_4 | H_2CO | C_2H_2 | SO | CN |
|---|----------------|----------------------------------|----------------------------------|----------------------------------|----------------------------------|----------------------------------|
| $10^{-6} \text{ M}_{\odot} \text{ yr}^{-1}$ | Smooth | $1.1\text{e+13} \text{ cm}^{-2}$ | $7.5\text{e+10} \text{ cm}^{-2}$ | $1.8\text{e+09} \text{ cm}^{-2}$ | $7.5\text{e+16} \text{ cm}^{-2}$ | $2.8\text{e+11} \text{ cm}^{-2}$ |
| f_{vol} | 0.05 | 0.2 | 0.4 | 0.05 | 0.2 | 0.4 |
| $f_{\text{ic}} = 0.1$ | 1.1e+00 | 1.1e+00 | 1.1e+00 | 1.5e+00 | 1.2e+00 | 0.05 |
| $f_{\text{ic}} = 0.3$ | 1.1e+00 | 1.1e+00 | 1.1e+00 | 1.3e+00 | 1.2e+00 | 1.3e+00 |
| $f_{\text{ic}} = 0.5$ | 1.1e+00 | 1.1e+00 | 1.2e+00 | 1.2e+00 | 1.2e+00 | 1.3e+00 |
| $10^{-5} \text{ M}_{\odot} \text{ yr}^{-1}$ | Smooth | $6.8\text{e+11} \text{ cm}^{-2}$ | $3.9\text{e+09} \text{ cm}^{-2}$ | $5.4\text{e+08} \text{ cm}^{-2}$ | $7.3\text{e+15} \text{ cm}^{-2}$ | $2.4\text{e+11} \text{ cm}^{-2}$ |
| f_{vol} | 0.05 | 0.2 | 0.4 | 0.05 | 0.2 | 0.4 |
| $f_{\text{ic}} = 0.1$ | 1.5e+00 | 1.3e+00 | 1.2e+00 | 3.4e+00 | 2.4e+00 | 1.9e+00 |
| $f_{\text{ic}} = 0.3$ | 1.2e+00 | 1.2e+00 | 1.2e+00 | 2.7e+00 | 2.0e+00 | 2.8e+00 |
| $f_{\text{ic}} = 0.5$ | 1.2e+00 | 1.2e+00 | 1.2e+00 | 2.1e+00 | 1.7e+00 | 2.3e+00 |
| $10^{-4} \text{ M}_{\odot} \text{ yr}^{-1}$ | Smooth | $2.3\text{e+10} \text{ cm}^{-2}$ | $2.5\text{e+08} \text{ cm}^{-2}$ | $9.1\text{e+07} \text{ cm}^{-2}$ | $6.4\text{e+14} \text{ cm}^{-2}$ | $5.5\text{e+10} \text{ cm}^{-2}$ |
| f_{vol} | 0.05 | 0.2 | 0.4 | 0.05 | 0.2 | 0.4 |
| $f_{\text{ic}} = 0.1$ | 3.7e+00 | 2.5e+00 | 1.9e+00 | 5.2e+00 | 4.2e+00 | 3.6e+00 |
| $f_{\text{ic}} = 0.3$ | 2.8e+00 | 1.9e+00 | 1.6e+00 | 4.5e+00 | 3.7e+00 | 3.3e+00 |
| $f_{\text{ic}} = 0.5$ | 2.0e+00 | 1.5e+00 | 1.4e+00 | 3.8e+00 | 3.4e+00 | 2.3e+00 |

Notes. The corresponding abundance profiles are shown in Fig. E.1. We note that the models with $f_{\text{vol}} = 0.2$, $l_* = 5 \times 10^{12} \text{ cm}$ and $f_{\text{vol}} = 0.4$, $l_* = 1 \times 10^{13} \text{ cm}$ have the same porosity length $h_* = 2.5 \times 10^{13} \text{ cm}$. Changes larger than one order of magnitude are in boldface.

Table E.3. Column density ratios relative to the smooth outflow for specific one-component outflows.

| \dot{M} | Species | CH_4 | H_2CO | C_2H_2 | SO | CN |
|---|----------------|----------------------------------|----------------------------------|----------------------------------|----------------------------------|----------------------------------|
| $10^{-6} \text{ M}_{\odot} \text{ yr}^{-1}$ | Smooth | $1.1\text{e+13} \text{ cm}^{-2}$ | $7.5\text{e+10} \text{ cm}^{-2}$ | $1.8\text{e+09} \text{ cm}^{-2}$ | $7.5\text{e+16} \text{ cm}^{-2}$ | $2.8\text{e+11} \text{ cm}^{-2}$ |
| f_{vol} | 0.05 | 0.2 | 0.4 | 0.05 | 0.2 | 0.4 |
| $f_{\text{ic}} = 0.1$ | 1.1e+00 | 1.1e+00 | 1.1e+00 | 1.5e+00 | 1.2e+00 | 0.05 |
| $f_{\text{ic}} = 0.3$ | 1.1e+00 | 1.1e+00 | 1.1e+00 | 1.3e+00 | 1.2e+00 | 1.3e+00 |
| $f_{\text{ic}} = 0.5$ | 1.1e+00 | 1.1e+00 | 1.2e+00 | 1.2e+00 | 1.2e+00 | 1.3e+00 |
| $10^{-5} \text{ M}_{\odot} \text{ yr}^{-1}$ | Smooth | $2.3\text{e+10} \text{ cm}^{-2}$ | $2.5\text{e+08} \text{ cm}^{-2}$ | $9.1\text{e+07} \text{ cm}^{-2}$ | $6.4\text{e+14} \text{ cm}^{-2}$ | $5.5\text{e+10} \text{ cm}^{-2}$ |
| f_{vol} | 0.05 | 0.2 | 0.4 | 0.05 | 0.2 | 0.4 |
| $f_{\text{ic}} = 0.1$ | 1.5e+00 | 1.3e+00 | 1.2e+00 | 3.4e+00 | 2.4e+00 | 1.9e+00 |
| $f_{\text{ic}} = 0.3$ | 1.2e+00 | 1.2e+00 | 1.2e+00 | 2.7e+00 | 2.0e+00 | 1.8e+00 |
| $f_{\text{ic}} = 0.5$ | 1.2e+00 | 1.2e+00 | 1.2e+00 | 2.1e+00 | 1.7e+00 | 1.6e+00 |
| $10^{-4} \text{ M}_{\odot} \text{ yr}^{-1}$ | Smooth | $2.3\text{e+10} \text{ cm}^{-2}$ | $2.5\text{e+08} \text{ cm}^{-2}$ | $9.1\text{e+07} \text{ cm}^{-2}$ | $6.4\text{e+14} \text{ cm}^{-2}$ | $5.5\text{e+10} \text{ cm}^{-2}$ |
| f_{vol} | 0.05 | 0.2 | 0.4 | 0.05 | 0.2 | 0.4 |
| $f_{\text{ic}} = 0.1$ | 3.7e+00 | 2.5e+00 | 1.9e+00 | 5.2e+00 | 4.2e+00 | 3.6e+00 |
| $f_{\text{ic}} = 0.3$ | 2.8e+00 | 1.9e+00 | 1.6e+00 | 4.5e+00 | 3.7e+00 | 3.3e+00 |
| $f_{\text{ic}} = 0.5$ | 2.0e+00 | 1.5e+00 | 1.4e+00 | 3.8e+00 | 3.4e+00 | 2.3e+00 |

Notes. The corresponding abundance profiles are shown in Fig. E.2. We note that models with $f_{\text{vol}} = 0.4$ have the same porosity length $h_* = 2.5 \times 10^{13} \text{ cm}$ as the one-component models with $f_{\text{vol}} = 0.2$, $l_* = 5 \times 10^{12} \text{ cm}$ and $f_{\text{vol}} = 0.4$, $l_* = 1 \times 10^{13} \text{ cm}$. Changes larger than one order of magnitude are in boldface.

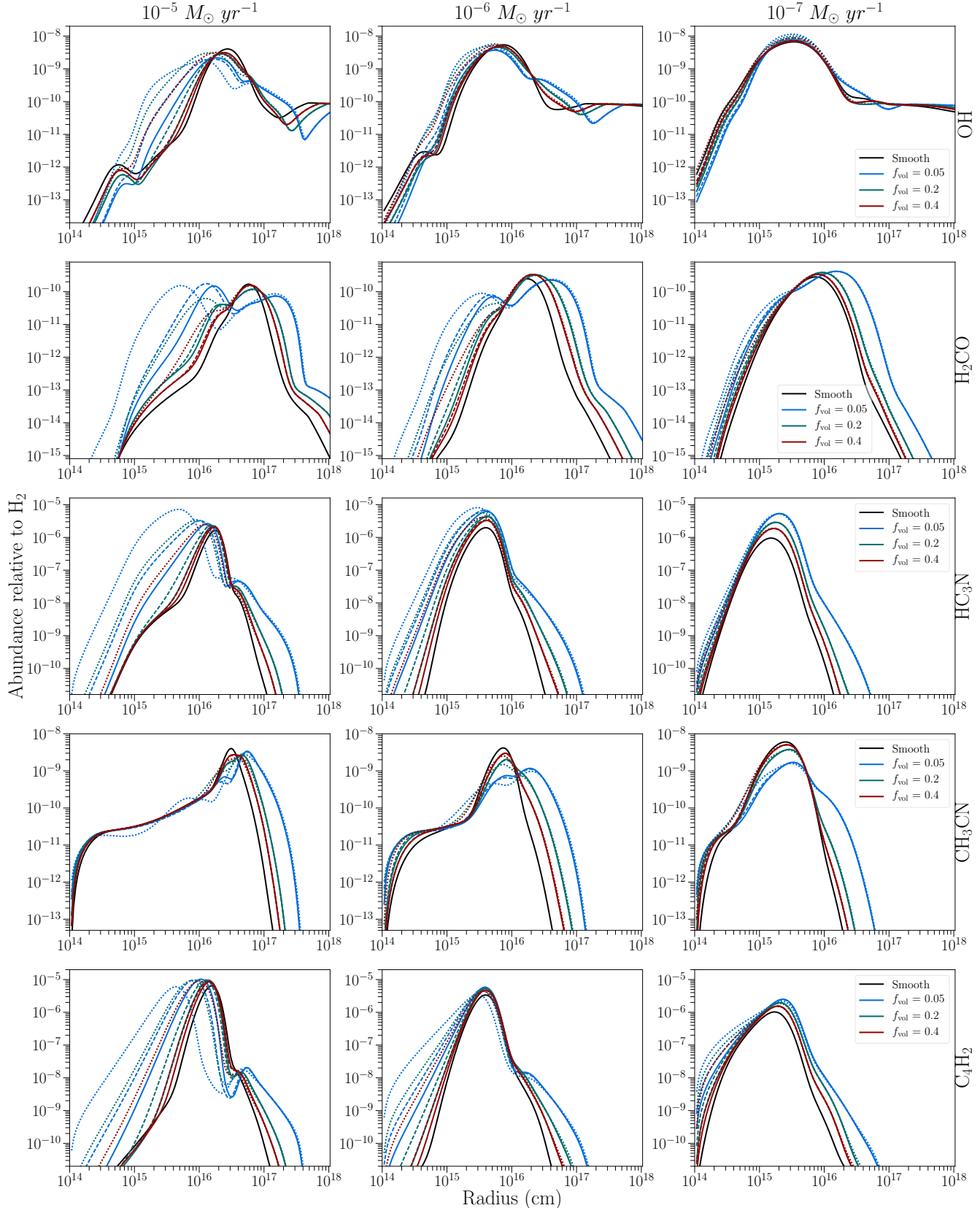


Fig. E.3. Abundance of OH, H₂CO, HC₃N, CH₃CN, and C₄H₂ relative to H₂ throughout a one-component C-rich outflow with different mass-loss rates \dot{M} and clump volume filling factors f_{vol} . Solid black line: calculated abundance for a smooth, uniform outflow. Solid coloured line: characteristic clump scale $l_* = 5 \times 10^{12} \text{ cm}$, porosity length $h_* = 1 \times 10^{14}, 2.5 \times 10^{13}, 1.25 \times 10^{13} \text{ cm}$ for $f_{\text{vol}} = 0.05, 0.2, 0.4$, respectively. Dashed coloured line: $l_* = 10^{13} \text{ cm}$, $h_* = 2 \times 10^{14}, 5 \times 10^{13}, 2.5 \times 10^{13} \text{ cm}$ for $f_{\text{vol}} = 0.05, 0.2, 0.4$, respectively. Dotted coloured line: $l_* = 5 \times 10^{13} \text{ cm}$, $h_* = 1 \times 10^{15}, 2.5 \times 10^{14}, 1.25 \times 10^{14} \text{ cm}$ for $f_{\text{vol}} = 0.05, 0.2, 0.4$, respectively. We note that models with $f_{\text{vol}} = 0.2$, $l_* = 5 \times 10^{12} \text{ cm}$ (green, solid) and $f_{\text{vol}} = 0.4$, $l_* = 1 \times 10^{13} \text{ cm}$ (red, dashed) have the same porosity length $h_* = 2.5 \times 10^{13} \text{ cm}$. For reference, $1 R_* = 5 \times 10^{13} \text{ cm}$.

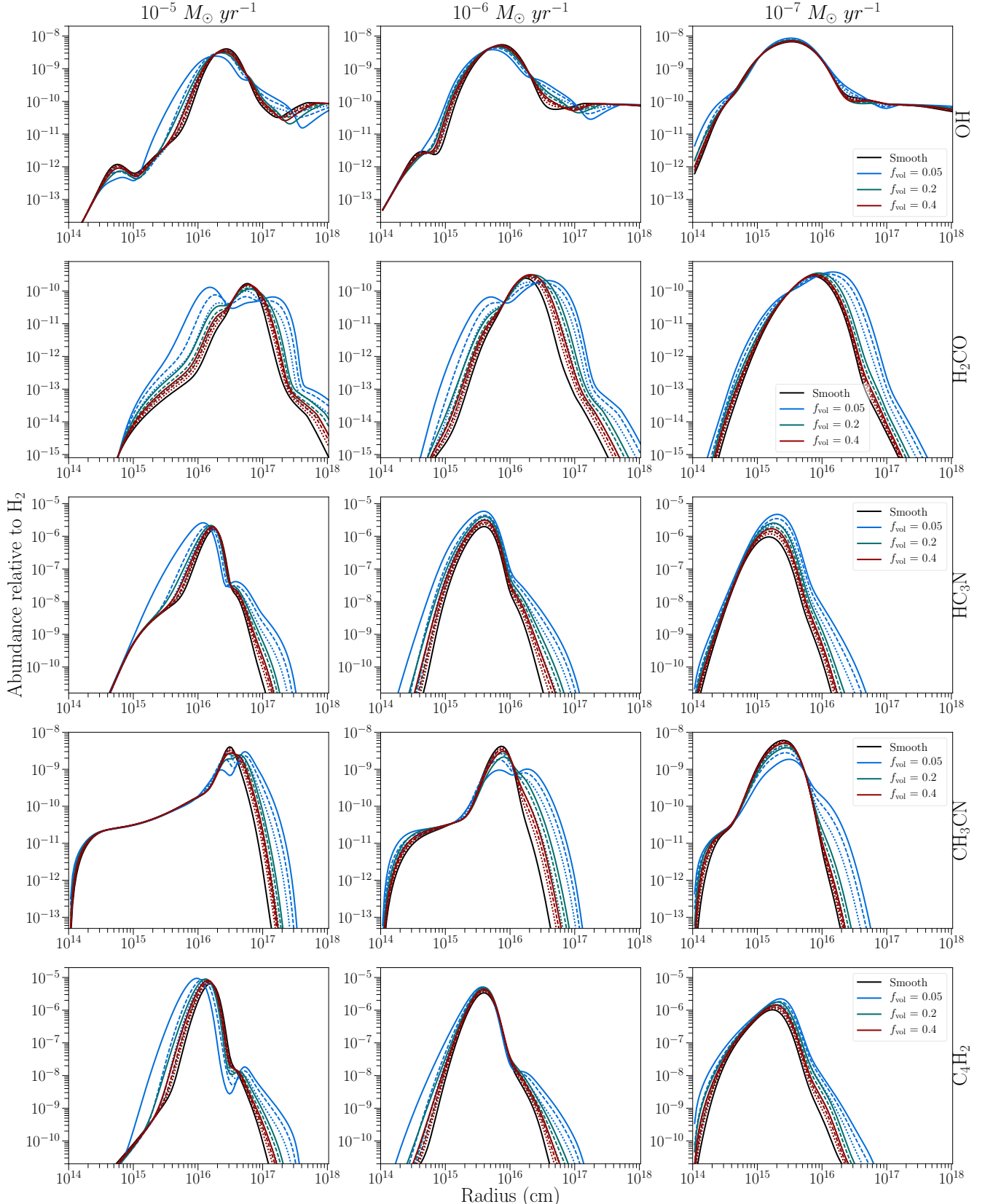


Fig. E.4. Abundance of OH, H₂CO, HC₃N, CH₃CN, and C₄H₂ relative to H₂ throughout a two-component C-rich outflow with different mass-loss rates \dot{M} and clump volume filling factors f_{vol} . The characteristic size of the clumps at the stellar radius is $l_* = 10^{13}$ cm. Blue lines: porosity length $h_* = 2 \times 10^{14}$ cm. Green lines: $h_* = 5 \times 10^{13}$ cm. Red lines: $h_* = 2.5 \times 10^{13}$ cm. Solid black line: calculated abundance for a smooth, uniform outflow. Solid coloured line: density contrast between the inter-clump and smooth outflow $f_{\text{ic}} = 0.1$. Dashed coloured line: $f_{\text{ic}} = 0.3$. Dotted coloured line: $f_{\text{ic}} = 0.5$. We note that the models with $f_{\text{vol}} = 0.4$ (red) have the same porosity length as the one-component outflows with $f_{\text{vol}} = 0.2$, $l_* = 5 \times 10^{12}$ cm and $f_{\text{vol}} = 0.4$, $l_* = 1 \times 10^{13}$ cm. For reference, $1 R_* = 5 \times 10^{13}$ cm.

Table E.3. Column density [cm^{-2}] of OH, H_2CO , HC_3N , CH_3CN , and C_4H_2 in a smooth C-rich outflow with different mass-loss rates, together with column density ratios relative to the smooth outflow for specific one-component outflows.

| \dot{M} | Species | OH | | H_2CO | | HC_3N | | CH_3CN | | C_4H_2 | | | | |
|--------------------------------------|------------------|------------------------------------|------------------------------------|--|------------------------------------|------------------------------------|------------------------------------|------------------------------------|------------------------------------|------------------------------------|------------------------------------|------------------------------------|------------------------------------|------------------------------------|
| | | Smooth | 1.3e+12 cm^{-2} | 2.1e+10 cm^{-2} | 0.05 | 0.2 | 0.4 | 0.05 | 0.2 | 0.4 | 0.05 | 0.2 | 0.4 | |
| $10^{-5} M_{\odot \text{ yr}^{-1}}$ | f_{vol} | Smooth | 0.05 | 0.2 | 0.4 | 0.05 | 0.2 | 0.4 | 0.05 | 0.2 | 0.4 | 0.05 | 0.2 | 0.4 |
| | I_* | $5 \times 10^{12} \text{ cm}$ | 9.4e-01 | 9.3e-01 | 1.2e+00 | 3.8e+00 | 1.4e+00 | 1.6e+00 | 9.9e-01 | 1.0e+00 | 1.0e+00 | 3.1e+00 | 1.8e+00 | 1.5e+00 |
| | I_* | $1 \times 10^{13} \text{ cm}$ | 1.1e+00 | 1.0e+00 | 1.5e+00 | 6.8e+00 | 1.3e+00 | 2.0e+00 | 9.8e-01 | 1.0e+00 | 1.0e+00 | 4.3e+00 | 2.2e+00 | 1.7e+00 |
| $10^{-6} M_{\odot \text{ yr}^{-1}}$ | I_* | $5 \times 10^{13} \text{ cm}$ | 2.8e+00 | 1.9e+00 | 1.7e+01 | 3.5e+00 | 1.7e+00 | 4.4e+01 | 9.3e-01 | 1.0e+00 | 1.0e+00 | 6.0e+00 | 4.7e+00 | 3.3e+00 |
| | f_{vol} | Smooth | 0.05 | 0.2 | 0.4 | 0.05 | 0.2 | 0.4 | 0.05 | 0.2 | 0.4 | 0.05 | 0.2 | 0.4 |
| | I_* | $5 \times 10^{12} \text{ cm}$ | 9.7e-01 | 1.0e+00 | 1.0e+00 | 1.6e+00 | 1.4e+00 | 1.3e+00 | 3.9e+00 | 2.2e+00 | 1.7e+00 | 5.4e-01 | 6.7e-01 | 1.9e+00 |
| $10^{-7} M_{\odot \text{ yr}^{-1}}$ | I_* | $1 \times 10^{13} \text{ cm}$ | 1.2e+00 | 1.1e+00 | 1.4e+00 | 2.1e+00 | 1.4e+00 | 2.6e+00 | 5.1e-01 | 1.8e+00 | 5.5e-01 | 2.1e+00 | 1.7e+00 | 1.4e+00 |
| | I_* | $5 \times 10^{13} \text{ cm}$ | 1.8e+00 | 2.0e+00 | 1.8e+00 | 3.4e+00 | 1.9e+00 | 4.8e+00 | 8.5e-01 | 3.1e+00 | 6.1e-01 | 9.0e-01 | 2.4e+00 | 2.1e+00 |
| | f_{vol} | Smooth | 0.05 | 0.2 | 0.4 | 0.05 | 0.2 | 0.4 | 0.05 | 0.2 | 0.4 | 0.05 | 0.2 | 0.4 |
| $10^{-8} M_{\odot \text{ yr}^{-1}}$ | I_* | $5 \times 10^{12} \text{ cm}$ | 9.4e-01 | 9.5e-01 | 9.8e-01 | 1.4e+00 | 1.3e+00 | 1.1e+00 | 4.3e+00 | 2.5e+00 | 1.8e+00 | 3.0e-01 | 6.4e-01 | 8.6e-01 |
| | I_* | $1 \times 10^{13} \text{ cm}$ | 1.1e+00 | 1.0e+00 | 1.0e+00 | 1.4e+00 | 1.3e+00 | 1.2e+00 | 4.3e+00 | 2.6e+00 | 3.1e-01 | 6.5e-01 | 8.7e-01 | 1.4e+00 |
| | I_* | $5 \times 10^{13} \text{ cm}$ | 1.4e+00 | 1.3e+00 | 1.3e+00 | 1.7e+00 | 1.5e+00 | 1.3e+00 | 4.0e+00 | 2.7e+00 | 3.8e-01 | 7.5e-01 | 9.6e-01 | 2.2e+00 |
| $10^{-9} M_{\odot \text{ yr}^{-1}}$ | f_{vol} | Smooth | 0.05 | 0.2 | 0.4 | 0.05 | 0.2 | 0.4 | 0.05 | 0.2 | 0.4 | 0.05 | 0.2 | 0.4 |
| | I_* | $5 \times 10^{12} \text{ cm}$ | 9.4e-01 | 9.5e-01 | 9.8e-01 | 1.4e+00 | 1.3e+00 | 1.1e+00 | 4.3e+00 | 2.5e+00 | 1.8e+00 | 3.0e-01 | 6.4e-01 | 8.6e-01 |
| | I_* | $1 \times 10^{13} \text{ cm}$ | 1.1e+00 | 1.0e+00 | 1.0e+00 | 1.4e+00 | 1.3e+00 | 1.2e+00 | 4.3e+00 | 2.6e+00 | 3.1e-01 | 6.5e-01 | 8.7e-01 | 1.4e+00 |
| $10^{-10} M_{\odot \text{ yr}^{-1}}$ | I_* | $5 \times 10^{12} \text{ cm}$ | 1.1e+00 | 1.1e+00 | 1.1e+00 | 1.7e+00 | 1.6e+00 | 1.4e+00 | 3.7e+00 | 1.7e+00 | 1.4e+00 | 1.0e+00 | 1.0e+00 | 1.5e+00 |
| | f_{vol} | Smooth | 0.05 | 0.2 | 0.4 | 0.05 | 0.2 | 0.4 | 0.05 | 0.2 | 0.4 | 0.05 | 0.2 | 0.4 |
| | f_{ic} | 0.1 | 1.4e+00 | 1.1e+00 | 1.1e+00 | 1.3e+00 | 1.2e+00 | 1.0e+00 | 3.7e+00 | 1.7e+00 | 1.4e+00 | 1.0e+00 | 1.0e+00 | 3.2e+00 |
| $10^{-11} M_{\odot \text{ yr}^{-1}}$ | f_{ic} | 0.3 | 1.2e+00 | 1.1e+00 | 1.2e+00 | 2.0e+00 | 1.2e+00 | 1.0e+00 | 3.7e+00 | 1.7e+00 | 1.4e+00 | 1.1e+00 | 1.1e+00 | 3.2e+00 |
| | f_{ic} | 0.5 | 1.1e+00 | 1.2e+00 | 1.3e+00 | 1.4e+00 | 1.1e+00 | 1.2e+00 | 3.7e+00 | 1.7e+00 | 1.3e+00 | 1.1e+00 | 1.1e+00 | 3.2e+00 |
| | f_{vol} | Smooth | 0.05 | 0.2 | 0.4 | 0.05 | 0.2 | 0.4 | 0.05 | 0.2 | 0.4 | 0.05 | 0.2 | 0.4 |
| $10^{-12} M_{\odot \text{ yr}^{-1}}$ | f_{vol} | 1.1e+00 | 1.1e+00 | 1.1e+00 | 1.7e+00 | 1.4e+00 | 1.3e+00 | 1.3e+00 | 4.0e+00 | 2.2e+00 | 1.7e+00 | 6.4e-01 | 7.3e-01 | 8.6e-01 |
| | f_{ic} | 0.1 | 1.2e+00 | 1.1e+00 | 1.1e+00 | 1.2e+00 | 1.3e+00 | 1.2e+00 | 2.6e+00 | 1.7e+00 | 1.4e+00 | 7.9e-01 | 8.9e-01 | 1.0e+00 |
| | f_{ic} | 0.3 | 1.1e+00 | 1.1e+00 | 1.2e+00 | 1.2e+00 | 1.1e+00 | 1.2e+00 | 2.6e+00 | 1.7e+00 | 1.4e+00 | 8.9e-01 | 9.9e-01 | 1.1e+00 |
| $10^{-13} M_{\odot \text{ yr}^{-1}}$ | f_{vol} | Smooth | 0.05 | 0.2 | 0.4 | 0.05 | 0.2 | 0.4 | 0.05 | 0.2 | 0.4 | 0.05 | 0.2 | 0.4 |
| | f_{ic} | 0.1 | 1.1e+00 | 1.1e+00 | 1.1e+00 | 1.2e+00 | 1.3e+00 | 1.2e+00 | 3.8e+00 | 2.3e+00 | 1.6e+00 | 3.5e-01 | 6.7e-01 | 8.8e-01 |
| | f_{ic} | 0.3 | 1.1e+00 | 1.1e+00 | 1.2e+00 | 1.2e+00 | 1.1e+00 | 1.2e+00 | 2.9e+00 | 1.8e+00 | 1.4e+00 | 5.4e-01 | 8.1e-01 | 9.9e-01 |
| $10^{-14} M_{\odot \text{ yr}^{-1}}$ | f_{vol} | Smooth | 0.05 | 0.2 | 0.4 | 0.05 | 0.2 | 0.4 | 0.05 | 0.2 | 0.4 | 0.05 | 0.2 | 0.4 |
| | f_{ic} | 0.1 | 1.1e+00 | 1.1e+00 | 1.1e+00 | 1.2e+00 | 1.3e+00 | 1.2e+00 | 3.8e+00 | 2.3e+00 | 1.6e+00 | 3.5e-01 | 6.7e-01 | 8.8e-01 |
| | f_{ic} | 0.3 | 1.1e+00 | 1.1e+00 | 1.2e+00 | 1.2e+00 | 1.1e+00 | 1.2e+00 | 2.9e+00 | 1.8e+00 | 1.4e+00 | 5.4e-01 | 8.1e-01 | 9.9e-01 |
| $10^{-15} M_{\odot \text{ yr}^{-1}}$ | f_{vol} | Smooth | 0.05 | 0.2 | 0.4 | 0.05 | 0.2 | 0.4 | 0.05 | 0.2 | 0.4 | 0.05 | 0.2 | 0.4 |
| | f_{ic} | 0.1 | 1.1e+00 | 1.1e+00 | 1.1e+00 | 1.2e+00 | 1.3e+00 | 1.2e+00 | 3.8e+00 | 2.3e+00 | 1.6e+00 | 3.5e-01 | 6.7e-01 | 8.8e-01 |
| | f_{ic} | 0.3 | 1.1e+00 | 1.1e+00 | 1.2e+00 | 1.2e+00 | 1.1e+00 | 1.2e+00 | 2.9e+00 | 1.8e+00 | 1.4e+00 | 5.4e-01 | 8.1e-01 | 9.9e-01 |

Notes. The corresponding abundance profiles are shown in Fig. E.3. We note that the models with $f_{\text{vol}} = 0.2$, $I_* = 5 \times 10^{12} \text{ cm}$ and $f_{\text{vol}} = 1 \times 10^{13} \text{ cm}$. Changes larger than one order of magnitude are in boldface.

Table E.4. Column density [cm^{-2}] of OH, H_2CO , HC_3N , CH_3CN , and C_4H_2 in a smooth C-rich outflow with different mass-loss rates, together with column density ratios relative to the smooth outflow for specific two-component outflows.

| \dot{M} | Species | OH | | H_2CO | | HC_3N | | CH_3CN | | C_4H_2 | |
|-------------------------------------|------------------|--------|--------------------------|--|--------------------------|-------------------------|-------------------------|--------------------------|-------------------------|-------------------------|--------------------------|
| | | Smooth | 1.3e+12 cm^{-2} | 2.1e+10 cm^{-2} | 0.05 | 0.2 | 0.4 | 0.05 | 0.2 | 0.4 | 0.05 |
| $10^{-5} M_{\odot \text{ yr}^{-1}}$ | f_{vol} | Smooth | 0.05 | 0.2 | 0.4 | 0.05 | 0.2 | 0.4 | 0.05 </ | | |

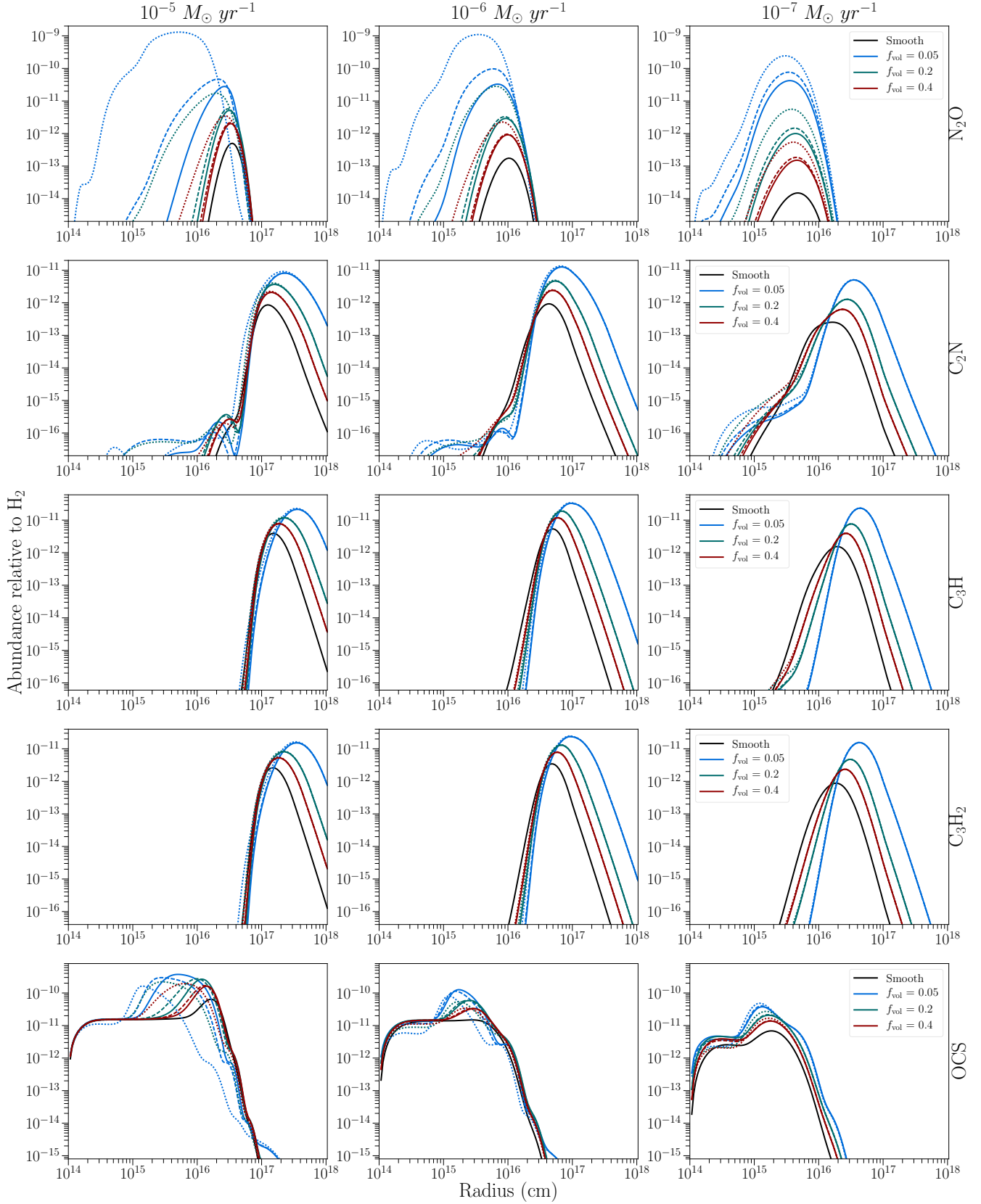


Fig. F.1. Abundance of N₂O, C₂N, C₃H, C₃H₂ and OCS relative to H₂ throughout a one-component O-rich outflow with different mass-loss rates \dot{M} and clump volume filling factors f_{vol} . Solid black line: calculated abundance for a smooth, uniform outflow. Solid coloured line: characteristic clump scale $l_* = 5 \times 10^{12} \text{ cm}$, porosity length $h_* = 1 \times 10^{14}, 2.5 \times 10^{13}, 1.25 \times 10^{13} \text{ cm}$ for $f_{\text{vol}} = 0.05, 0.2, 0.4$, respectively. Dashed coloured line: $l_* = 10^{13} \text{ cm}$, $h_* = 2 \times 10^{14}, 5 \times 10^{13}, 2.5 \times 10^{13} \text{ cm}$ for $f_{\text{vol}} = 0.05, 0.2, 0.4$, respectively. Dotted coloured line: $l_* = 5 \times 10^{13} \text{ cm}$, $h_* = 1 \times 10^{15}, 2.5 \times 10^{14}, 1.25 \times 10^{14} \text{ cm}$ for $f_{\text{vol}} = 0.05, 0.2, 0.4$, respectively. We note that models with $f_{\text{vol}} = 0.2$, $l_* = 5 \times 10^{12} \text{ cm}$ (green, solid) and $f_{\text{vol}} = 0.4$, $l_* = 1 \times 10^{13} \text{ cm}$ (red, dashed) have the same porosity length $h_* = 2.5 \times 10^{13} \text{ cm}$. For reference, $1 R_* = 5 \times 10^{13} \text{ cm}$.

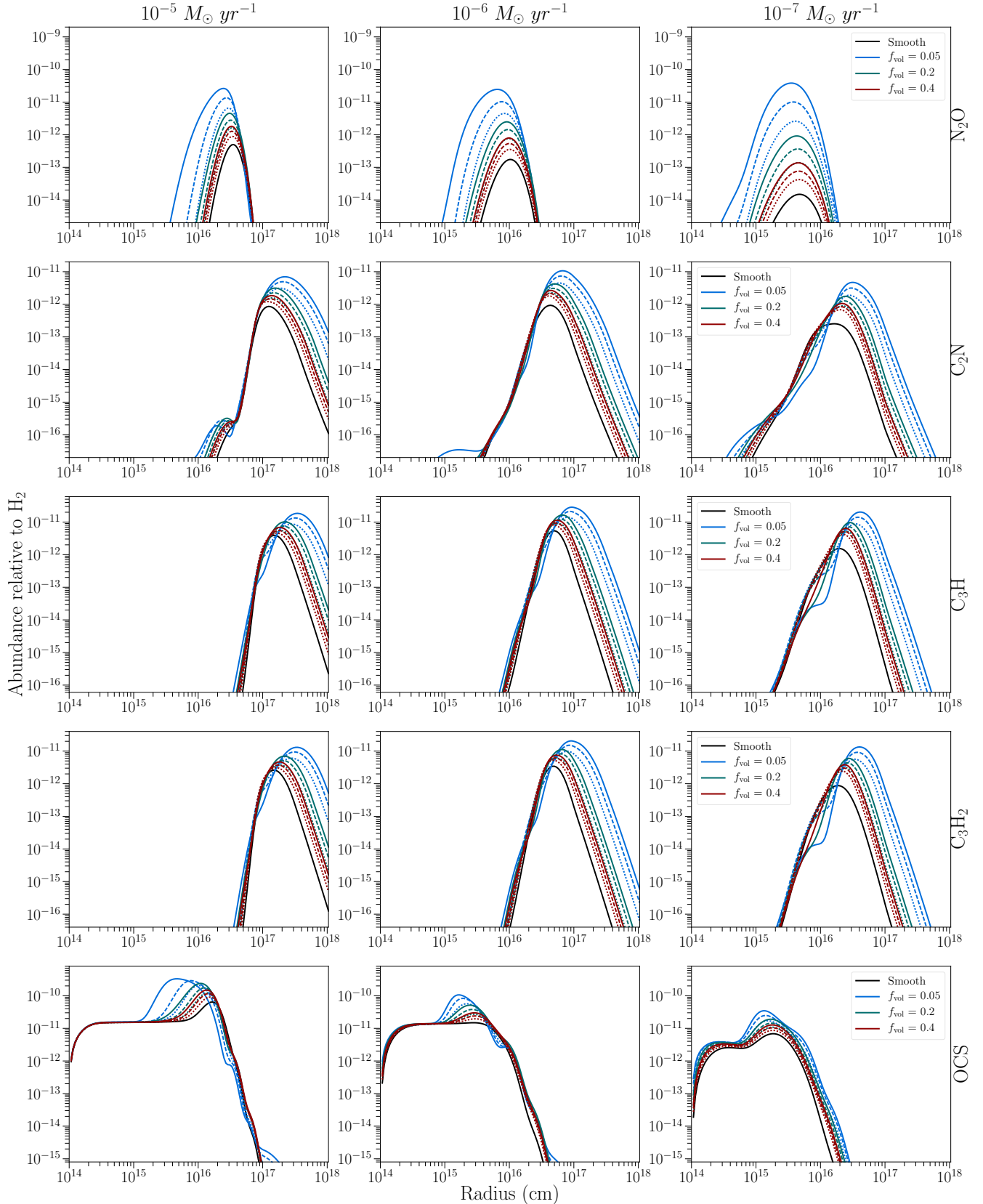


Fig. F.2. Abundance of N₂O, C₂N, C₃H, C₃H₂ and OCS relative to H₂ throughout a two-component O-rich outflow with different mass-loss rates \dot{M} and clump volume filling factors f_{vol} . The characteristic size of the clumps at the stellar radius is $l_* = 10^{13}$ cm. Blue lines: porosity length $h_* = 2 \times 10^{14}$ cm. Green lines: $h_* = 5 \times 10^{13}$ cm. Red lines: $h_* = 2.5 \times 10^{13}$ cm. Solid black line: calculated abundance for a smooth, uniform outflow. Solid coloured line: density contrast between the inter-clump and smooth outflow $f_{\text{ic}} = 0.1$. Dashed coloured line: $f_{\text{ic}} = 0.3$. Dotted coloured line: $f_{\text{ic}} = 0.5$. We note that the models with $f_{\text{vol}} = 0.4$ (red) have the same porosity length as the one-component outflows with $f_{\text{vol}} = 0.2$, $l_* = 5 \times 10^{12}$ cm and $f_{\text{vol}} = 0.4$, $l_* = 1 \times 10^{13}$ cm. For reference, $1 R_* = 5 \times 10^{13}$ cm.

Table F.1. Column density [cm^{-2}] of N_2O , C_2N , C_3H , C_3H_2 and OCS in a smooth O-rich outflow with different mass-loss rates, together with column density ratios relative to the smooth outflow for specific one-component outflows.

| M | Species | N_2O | | C_2N | | C_3H | | C_3H_2 | | OCS | |
|-------------------------------------|------------------|----------------------|---------------------------|---------------------------|-----------|----------------------|-----------|------------------------|-----------|-----------|-----------|
| | | f_{vol} | $6.4e+07 \text{ cm}^{-2}$ | $4.1e+07 \text{ cm}^{-2}$ | 0.05 | 0.2 | 0.4 | 0.05 | 0.2 | 0.4 | 0.05 |
| $10^{-5} M_{\odot} \text{ yr}^{-1}$ | f_{vol} | 0.05 | 0.2 | 0.4 | 0.05 | 0.2 | 0.4 | 0.05 | 0.2 | 0.4 | 0.05 |
| $I_* = 5 \times 10^{12} \text{ cm}$ | $1.2e+02$ | $1.2e+01$ | $4.4e+00$ | $8.2e+00$ | $4.2e+00$ | $2.4e+00$ | $3.6e+00$ | $2.7e+00$ | $1.9e+00$ | $3.9e+00$ | $2.8e+00$ |
| $I_* = 1 \times 10^{13} \text{ cm}$ | $4.4e+02$ | $1.5e+01$ | $4.9e+00$ | $8.6e+00$ | $4.3e+00$ | $2.4e+00$ | $3.7e+00$ | $2.7e+00$ | $1.9e+00$ | $4.0e+00$ | $2.8e+00$ |
| $I_* = 5 \times 10^{13} \text{ cm}$ | $7.8e+04$ | $1.6e+02$ | $1.3e+01$ | $1.1e+01$ | $5.2e+00$ | $2.8e+00$ | $4.2e+00$ | $3.0e+00$ | $2.1e+00$ | $4.6e+00$ | $3.2e+00$ |
| $10^{-6} M_{\odot} \text{ yr}^{-1}$ | f_{vol} | 0.05 | 0.2 | 0.4 | 0.05 | 0.2 | 0.4 | 0.05 | 0.2 | 0.4 | 0.05 |
| $I_* = 5 \times 10^{12} \text{ cm}$ | $4.2e+02$ | $2.0e+01$ | $5.5e+00$ | $1.0e+01$ | $4.0e+00$ | $2.2e+00$ | $4.6e+00$ | $2.9e+00$ | $1.9e+00$ | $5.1e+00$ | $3.1e+00$ |
| $I_* = 1 \times 10^{13} \text{ cm}$ | $1.8e+03$ | $2.4e+01$ | $6.0e+00$ | $1.0e+01$ | $4.1e+00$ | $2.2e+00$ | $4.6e+00$ | $3.0e+00$ | $1.9e+00$ | $5.2e+00$ | $3.2e+00$ |
| $I_* = 5 \times 10^{13} \text{ cm}$ | $3.8e+04$ | $4.1e+02$ | $2.1e+01$ | $1.2e+01$ | $4.4e+00$ | $2.3e+00$ | $5.0e+00$ | $3.2e+00$ | $2.0e+00$ | $5.6e+00$ | $3.4e+00$ |
| $10^{-7} M_{\odot} \text{ yr}^{-1}$ | f_{vol} | 0.05 | 0.2 | 0.4 | 0.05 | 0.2 | 0.4 | 0.05 | 0.2 | 0.4 | 0.05 |
| $I_* = 5 \times 10^{12} \text{ cm}$ | $3.9e+03$ | $7.0e+01$ | $1.0e+01$ | $6.1e+00$ | $2.3e+00$ | $1.5e+00$ | $5.5e+00$ | $2.4e+00$ | $1.6e+00$ | $6.6e+00$ | $2.7e+00$ |
| $I_* = 1 \times 10^{13} \text{ cm}$ | $7.5e+03$ | $1.1e+02$ | $1.3e+01$ | $6.2e+00$ | $2.3e+00$ | $1.5e+00$ | $5.6e+00$ | $2.4e+00$ | $1.6e+00$ | $6.6e+00$ | $2.7e+00$ |
| $I_* = 5 \times 10^{13} \text{ cm}$ | $2.8e+04$ | $5.0e+02$ | $4.5e+01$ | $6.4e+00$ | $2.3e+00$ | $1.6e+00$ | $5.7e+00$ | $2.4e+00$ | $1.6e+00$ | $6.8e+00$ | $2.7e+00$ |

Table F.2. Column density [cm^{-2}] of N_2O , C_2N , C_3H , C_3H_2 and OCS in a smooth O-rich outflow with different mass-loss rates, together with column density ratios relative to the smooth outflow for specific two-component outflows.

| M | Species | N_2O | | C_2N | | C_3H | | C_3H_2 | | OCS | |
|-------------------------------------|------------------|----------------------|---------------------------|---------------------------|-----------|----------------------|-----------|------------------------|-----------|-----------|-----------|
| | | f_{vol} | $6.4e+07 \text{ cm}^{-2}$ | $4.1e+07 \text{ cm}^{-2}$ | 0.05 | 0.2 | 0.4 | 0.05 | 0.2 | 0.4 | 0.05 |
| $10^{-5} M_{\odot} \text{ yr}^{-1}$ | f_{vol} | 0.05 | 0.2 | 0.4 | 0.05 | 0.2 | 0.4 | 0.05 | 0.2 | 0.4 | 0.05 |
| $f_{\text{ic}} = 0.1$ | $1.2e+02$ | $1.2e+01$ | $4.1e+00$ | $7.3e+00$ | $3.7e+00$ | $2.3e+00$ | $3.2e+00$ | $2.4e+00$ | $1.7e+00$ | $3.5e+00$ | $2.5e+00$ |
| $f_{\text{ic}} = 0.3$ | $4.5e+01$ | $6.5e+00$ | $2.8e+00$ | $5.4e+00$ | $2.8e+00$ | $1.9e+00$ | $2.7e+00$ | $1.9e+00$ | $1.6e+00$ | $6.6e+00$ | $2.5e+00$ |
| $f_{\text{ic}} = 0.5$ | $1.7e+01$ | $3.6e+00$ | $1.9e+00$ | $3.8e+00$ | $2.1e+00$ | $1.7e+00$ | $2.1e+00$ | $1.6e+00$ | $1.5e+00$ | $2.5e+00$ | $2.3e+00$ |
| $10^{-6} M_{\odot} \text{ yr}^{-1}$ | f_{vol} | 0.05 | 0.2 | 0.4 | 0.05 | 0.2 | 0.4 | 0.05 | 0.2 | 0.4 | 0.05 |
| $f_{\text{ic}} = 0.1$ | $3.4e+02$ | $1.7e+01$ | $4.9e+00$ | $8.7e+00$ | $3.9e+00$ | $2.6e+00$ | $4.1e+00$ | $2.8e+00$ | $2.1e+00$ | $6.4e+00$ | $2.9e+00$ |
| $f_{\text{ic}} = 0.3$ | $1.0e+02$ | $9.4e+00$ | $3.3e+00$ | $6.2e+00$ | $3.0e+00$ | $2.2e+00$ | $3.3e+00$ | $2.3e+00$ | $1.9e+00$ | $3.6e+00$ | $2.4e+00$ |
| $f_{\text{ic}} = 0.5$ | $3.5e+01$ | $4.7e+00$ | $2.2e+00$ | $4.2e+00$ | $2.0e+00$ | $2.0e+00$ | $2.6e+00$ | $2.0e+00$ | $1.8e+00$ | $2.8e+00$ | $2.0e+00$ |
| $10^{-7} M_{\odot} \text{ yr}^{-1}$ | f_{vol} | 0.05 | 0.2 | 0.4 | 0.05 | 0.2 | 0.4 | 0.05 | 0.2 | 0.4 | 0.05 |
| $f_{\text{ic}} = 0.1$ | $3.6e+03$ | $6.7e+01$ | $9.5e+00$ | $2.3e+00$ | $3.0e+00$ | $2.7e+00$ | $5.3e+00$ | $3.2e+00$ | $2.5e+00$ | $6.4e+00$ | $3.5e+00$ |
| $f_{\text{ic}} = 0.3$ | $8.5e+02$ | $2.5e+01$ | $5.2e+00$ | $4.5e+00$ | $2.5e+00$ | $2.1e+00$ | $4.1e+00$ | $2.7e+00$ | $2.3e+00$ | $4.8e+00$ | $2.9e+00$ |
| $f_{\text{ic}} = 0.5$ | $2.0e+02$ | $9.2e+00$ | $2.9e+00$ | $3.2e+00$ | $2.1e+00$ | $2.0e+00$ | $3.1e+00$ | $2.4e+00$ | $2.3e+00$ | $3.5e+00$ | $2.5e+00$ |

Notes. Corresponding abundance profiles are shown in Fig. F.3. We note that the models with $f_{\text{vol}} = 0.2$, $I_* = 5 \times 10^{12} \text{ cm}$ and $f_{\text{vol}} = 0.4$, $I_* = 1 \times 10^{13} \text{ cm}$ have the same porosity length $h_* = 2.5 \times 10^{13} \text{ cm}$. Differences larger than one order of magnitude are in boldface.

Notes. Corresponding abundance profiles are shown in Fig. F.4. We note that models with $f_{\text{vol}} = 0.4$ have the same porosity length $h_* = 2.5 \times 10^{13} \text{ cm}$ as the one-component models with $f_{\text{vol}} = 0.2$, $I_* = 5 \times 10^{12} \text{ cm}$ and $f_{\text{vol}} = 0.4$, $I_* = 1 \times 10^{13} \text{ cm}$. Differences larger than one order of magnitude are in boldface.

Table A&A 634, C1 (2020)

| M | Species | N_2O | | C_2N | | C_3H | | C_3H_2 | | OCS | |
|-------------------------------------|------------------|----------------------|---------------------------|---------------------------|-----------|----------------------|-----------|------------------------|-----------|-----------|-----------|
| | | f_{vol} | $6.4e+07 \text{ cm}^{-2}$ | $4.1e+07 \text{ cm}^{-2}$ | 0.05 | 0.2 | 0.4 | 0.05 | 0.2 | 0.4 | 0.05 |
| $10^{-5} M_{\odot} \text{ yr}^{-1}$ | f_{vol} | 0.05 | 0.2 | 0.4 | 0.05 | 0.2 | 0.4 | 0.05 | 0.2 | 0.4 | 0.05 |
| $f_{\text{ic}} = 0.1$ | $1.2e+02$ | $1.2e+01$ | $4.1e+00$ | $7.3e+00$ | $3.7e+00$ | $2.3e+00$ | $3.2e+00$ | $2.4e+00$ | $1.7e+00$ | $3.5e+00$ | $2.5e+00$ |
| $f_{\text{ic}} = 0.3$ | $4.5e+01$ | $6.5e+00$ | $2.8e+00$ | $5.4e+00$ | $2.8e+00$ | $1.9e+00$ | $2.7e+00$ | $1.9e+00$ | $1.6e+00$ | $6.6e+00$ | $2.5e+00$ |
| $f_{\text{ic}} = 0.5$ | $1.7e+01$ | $3.6e+00$ | $1.9e+00$ | $3.8e+00$ | $2.1e+00$ | $1.7e+00$ | $2.1e+00$ | $1.6e+00$ | $1.5e+00$ | $2.5e+00$ | $2.3e+00$ |
| $10^{-6} M_{\odot} \text{ yr}^{-1}$ | f_{vol} | 0.05 | 0.2 | 0.4 | 0.05 | 0.2 | 0.4 | 0.05 | 0.2 | 0.4 | 0.05 |
| $f_{\text{ic}} = 0.1$ | $3.4e+02$ | $1.7e+01$ | $4.9e+00$ | $8.7e+00$ | $3.9e+00$ | $2.6e+00$ | $4.1e+00$ | $2.8e+00$ | $2.1e+00$ | $6.4e+00$ | $2.9e+00$ |
| $f_{\text{ic}} = 0.3$ | $1.0e+02$ | $9.4e+00$ | $3.3e+00$ | $6.2e+00$ | $3.0e+00$ | $2.2e+00$ | $3.3e+00$ | $2.3e+00$ | $1.9e+00$ | $6.6e+00$ | $2.9e+00$ |
| $f_{\text{ic}} = 0.5$ | $3.5e+01$ | $4.7e+00$ | $2.2e+00$ | $4.2e+00$ | $2.0e+00$ | $2.0e+00$ | $2.6e+00$ | $2.0e+00$ | $1.8e+00$ | $2.8e+00$ | $2.0e+00$ |
| $10^{-7} M_{\odot} \text{ yr}^{-1}$ | f_{vol} | 0.05 | 0.2 | 0.4 | 0.05 | 0.2 | 0.4 | 0.05 | 0.2 | 0.4 | 0.05 |
| $f_{\text{ic}} = 0.1$ | $3.6e+03$ | $6.7e+01$ | $9.5e+00$ | $2.3e+00$ | $3.0e+00$ | $2.7e+00$ | $5.3e+00$ | $3.2e+00$ | $2.5e+00$ | $6.4e+00$ | $3.5e+00$ |
| $f_{\text{ic}} = 0.3$ | $8.5e+02$ | $2.5e+01$ | $5.2e+00$ | $4.5e+00$ | $2.5e+00$ | $2.1e+00$ | $4.1e+00$ | $2.7e+00$ | $2.3e+00$ | $4.8e+00$ | $2.9e+00$ |
| $f_{\text{ic}} = 0.5$ | $2.0e+02$ | $9.2e+00$ | $2.9e+00$ | $3.2e+00$ | $2.1e+00$ | $2.0e+00$ | $3.1e+00$ | $2.4e+00$ | $2.3e+00$ | $3.5e+00$ | $2.5e+00$ |

Notes. Corresponding abundance profiles are shown in Fig. F.4. We note that models with $f_{\text{vol}} = 0.4$ have the same porosity length $h_* = 2.5 \times 10^{13} \text{ cm}$ as the one-component models with $f_{\text{vol}} = 0.2$, $I_* = 5 \times 10^{12} \text{ cm}$ and $f_{\text{vol}} = 0.4$, $I_* = 1 \times 10^{13} \text{ cm}$. Differences larger than one order of magnitude are in boldface.

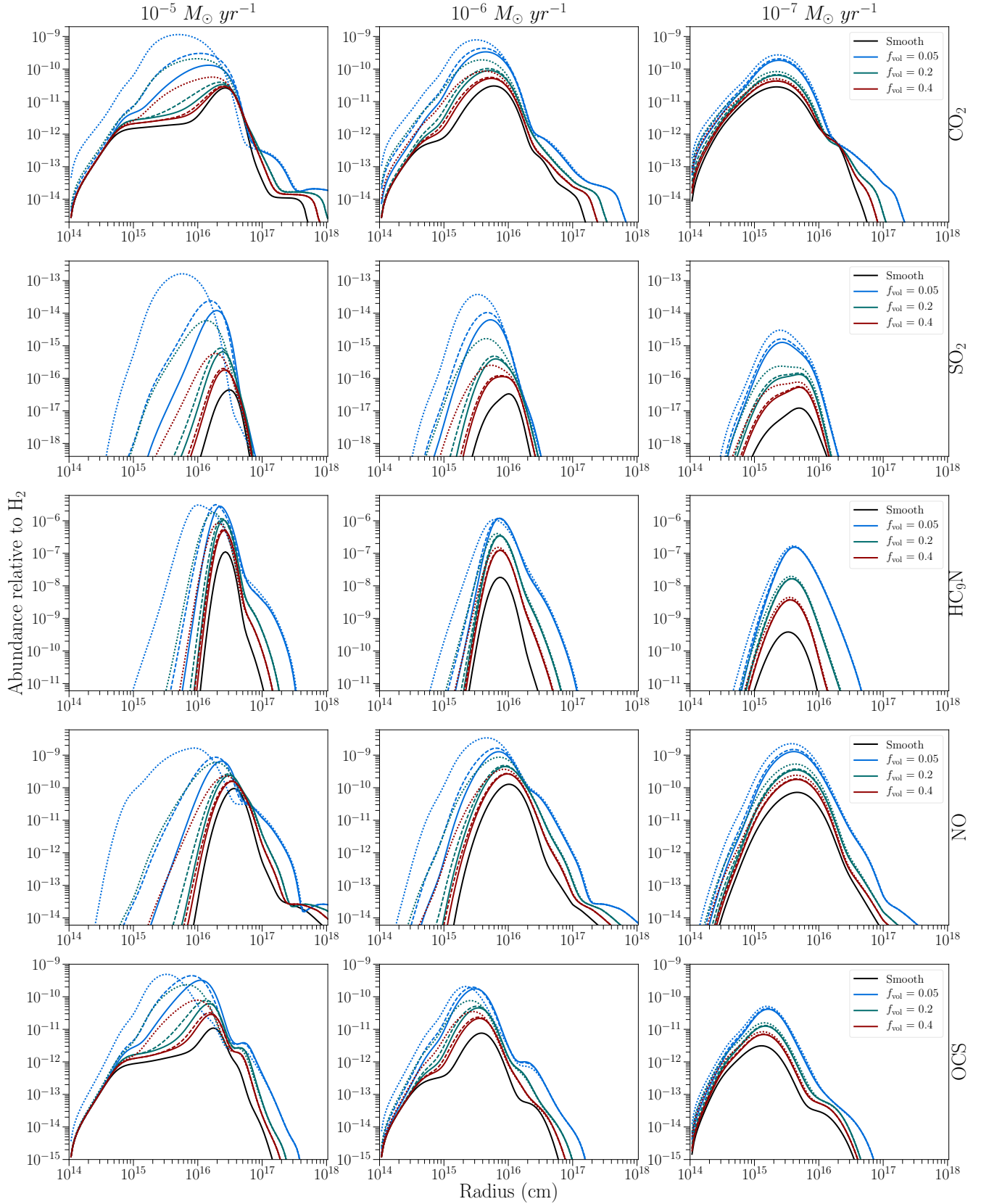


Fig. F.3. Abundance of CO_2 , SO_2 , HC_9N , NO , and OCS relative to H_2 throughout a one-component C-rich outflow with different mass-loss rates \dot{M} and clump volume filling factors f_{vol} . Solid black line: calculated abundance for a smooth, uniform outflow. Solid coloured line: characteristic clump scale $l_* = 5 \times 10^{12} \text{ cm}$, porosity length $h_* = 1 \times 10^{14}, 2.5 \times 10^{13}, 1.25 \times 10^{13} \text{ cm}$ for $f_{\text{vol}} = 0.05, 0.2, 0.4$, respectively. Dashed coloured line: $l_* = 10^{13} \text{ cm}$, $h_* = 2 \times 10^{14}, 5 \times 10^{13}, 2.5 \times 10^{13} \text{ cm}$ for $f_{\text{vol}} = 0.05, 0.2, 0.4$, respectively. Dotted coloured line: $l_* = 5 \times 10^{13} \text{ cm}$, $h_* = 1 \times 10^{15}, 2.5 \times 10^{14}, 1.25 \times 10^{14} \text{ cm}$ for $f_{\text{vol}} = 0.05, 0.2, 0.4$, respectively. We note that models with $f_{\text{vol}} = 0.2$, $l_* = 5 \times 10^{12} \text{ cm}$ (green, solid) and $f_{\text{vol}} = 0.4$, $l_* = 1 \times 10^{13} \text{ cm}$ (red, dashed) have the same porosity length $h_* = 2.5 \times 10^{13} \text{ cm}$. For reference, $1 R_* = 5 \times 10^{13} \text{ cm}$.

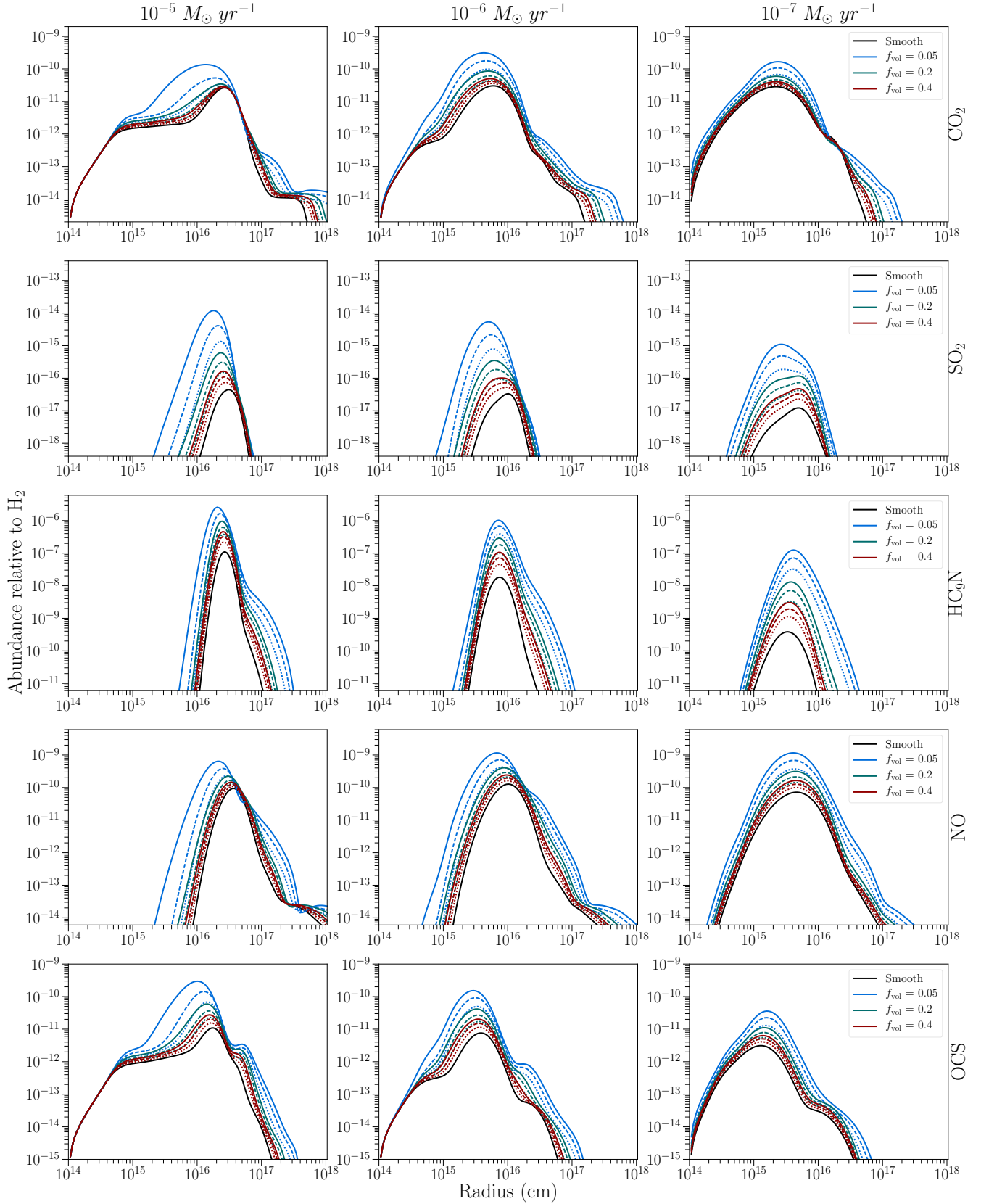


Fig. F.4. Abundance of CO_2 , SO_2 , HC_9N , NO , and OCS relative to H_2 throughout a two-component C-rich outflow with different mass-loss rates \dot{M} and clump volume filling factors f_{vol} . The characteristic size of the clumps at the stellar radius is $l_* = 10^{13} \text{ cm}$. Blue lines: porosity length $h_* = 2 \times 10^{14} \text{ cm}$. Green lines: $h_* = 5 \times 10^{13} \text{ cm}$. Red lines: $h_* = 2.5 \times 10^{13} \text{ cm}$. Solid black line: calculated abundance for a smooth, uniform outflow. Solid coloured line: density contrast between the inter-clump and smooth outflow $f_{\text{ic}} = 0.1$. Dashed coloured line: $f_{\text{ic}} = 0.3$. Dotted coloured line: $f_{\text{ic}} = 0.5$. We note that the models with $f_{\text{vol}} = 0.4$ (red) have the same porosity length as the one-component outflows with $f_{\text{vol}} = 0.2$, $l_* = 5 \times 10^{12} \text{ cm}$ and $f_{\text{vol}} = 0.4$, $l_* = 1 \times 10^{13} \text{ cm}$. For reference, $1 R_* = 5 \times 10^{13} \text{ cm}$.

Table F.3. Column density [cm^{-2}] of CO_2 , SO_2 , HC_9N , NO , and OCS in a smooth C-rich outflow with different mass-loss rates, together with column density ratios relative to the smooth outflow for specific one-component outflows.

| \dot{M} | Species | CO_2 | SO_2 | HC_9N | NO | OCS |
|-------------------------------------|-----------------------------|---------------------------|---------------------------|-----------------------------|-----------------------------|-----------------------------|
| Smooth | | $3.6e+10 \text{ cm}^{-2}$ | $8.4e+03 \text{ cm}^{-2}$ | $1.5e+13 \text{ cm}^{-2}$ | $1.5e+10 \text{ cm}^{-2}$ | $2.0e+10 \text{ cm}^{-2}$ |
| f_{vol} | 0.05 | 0.2 | 0.4 | 0.05 | 0.2 | 0.4 |
| $I_* = 5 \times 10^{12} \text{ cm}$ | $6.7e+00$ | $1.7e+00$ | $1.3e+00$ | $3.5e+01$ | $1.0e+01$ | $4.8e+00$ |
| $I_* = 1 \times 10^{13} \text{ cm}$ | $1.9e+01$ | $2.0e+00$ | $1.4e+00$ | $5.3e+01$ | $1.3e+01$ | $5.4e+00$ |
| $I_* = 5 \times 10^{13} \text{ cm}$ | $1.1e+02$ | $1.6e-01$ | $3.6e-00$ | $1.4e+02$ | $2.9e-01$ | $1.2e+01$ |
| f_{vol} | 0.05 | 0.2 | 0.4 | 0.05 | 0.2 | 0.4 |
| $I_* = 5 \times 10^{12} \text{ cm}$ | $1.5e+01$ | $3.5e+00$ | $1.9e+00$ | $3.5e+02$ | $1.8e+01$ | $6.5e+00$ |
| $I_* = 1 \times 10^{13} \text{ cm}$ | $2.1e+01$ | $4.5e+00$ | $2.2e+00$ | $7.2e+02$ | $2.4e+01$ | $9.6e+00$ |
| $I_* = 5 \times 10^{13} \text{ cm}$ | $4.9e+01$ | $1.2e+01$ | $4.9e+00$ | $3.7e+03$ | $1.4e+02$ | $9.2e+00$ |
| Smooth | | $7.3e+09 \text{ cm}^{-2}$ | $2.6e+03 \text{ cm}^{-2}$ | $1.3e+12 \text{ cm}^{-2}$ | $1.1e+10 \text{ cm}^{-2}$ | $2.3e+09 \text{ cm}^{-2}$ |
| f_{vol} | 0.05 | 0.2 | 0.4 | 0.05 | 0.2 | 0.4 |
| $I_* = 5 \times 10^{12} \text{ cm}$ | $1.5e+00$ | $3.5e+00$ | $1.9e+00$ | $3.5e+02$ | $1.8e+01$ | $6.6e+00$ |
| $I_* = 1 \times 10^{13} \text{ cm}$ | $2.1e+00$ | $4.5e+00$ | $2.2e+00$ | $7.2e+02$ | $1.9e+01$ | $6.9e+00$ |
| $I_* = 5 \times 10^{13} \text{ cm}$ | $4.9e+00$ | $1.2e+01$ | $4.9e+00$ | $1.4e+02$ | $1.8e+01$ | $9.7e+00$ |
| Smooth | | $2.6e+09 \text{ cm}^{-2}$ | $3.0e+02 \text{ cm}^{-2}$ | $9.3e+09 \text{ cm}^{-2}$ | $2.2e+09 \text{ cm}^{-2}$ | $3.4e+08 \text{ cm}^{-2}$ |
| f_{vol} | 0.05 | 0.2 | 0.4 | 0.05 | 0.2 | 0.4 |
| $I_* = 5 \times 10^{12} \text{ cm}$ | $4.6e+00$ | $2.0e+00$ | $1.4e+00$ | $1.5e+02$ | $1.6e+01$ | $2.8e+00$ |
| $I_* = 1 \times 10^{13} \text{ cm}$ | $5.2e+00$ | $2.1e+00$ | $1.5e+00$ | $1.9e+02$ | $1.9e+01$ | $3.0e+00$ |
| $I_* = 5 \times 10^{13} \text{ cm}$ | $7.3e+00$ | $2.9e+00$ | $1.9e+00$ | $3.7e+02$ | $4.0e+01$ | $3.6e+00$ |

Notes. Corresponding abundance profiles are shown in Fig. F.3. We note that the models with $f_{\text{vol}} = 0.2$, $I_* = 5 \times 10^{12} \text{ cm}$ and $f_{\text{vol}} = 0.4$, $I_* = 1 \times 10^{13} \text{ cm}$ have the same porosity length $h_* = 2.5 \times 10^{13} \text{ cm}$. Differences larger than one order of magnitude are in boldface.

Table F.4. Column density [cm^{-2}] of CO_2 , SO_2 , HC_9N , NO , and OCS in a smooth C-rich outflow with different mass-loss rates, together with column density ratios relative to the smooth outflow for specific two-component outflows.

| \dot{M} | Species | CO_2 | SO_2 | HC_9N | NO | OCS |
|-----------------------|-----------|---------------------------|---------------------------|-----------------------------|---------------------------|---------------------------|
| Smooth | | $3.6e+10 \text{ cm}^{-2}$ | $8.4e+03 \text{ cm}^{-2}$ | $1.5e+13 \text{ cm}^{-2}$ | $1.5e+10 \text{ cm}^{-2}$ | $2.0e+10 \text{ cm}^{-2}$ |
| f_{vol} | 0.05 | 0.2 | 0.4 | 0.05 | 0.2 | 0.4 |
| $f_{\text{ic}} = 0.1$ | $6.4e+00$ | $1.7e+00$ | $1.3e+00$ | $5.2e+02$ | $1.7e+01$ | $4.5e+00$ |
| $f_{\text{ic}} = 0.3$ | $2.4e+00$ | $1.4e+00$ | $1.2e+00$ | $1.3e+02$ | $2.8e+00$ | $6.3e+00$ |
| $f_{\text{ic}} = 0.5$ | $1.6e+00$ | $1.3e+00$ | $1.2e+00$ | $3.6e+01$ | $3.9e+00$ | $9.9e+00$ |
| Smooth | | $7.3e+09 \text{ cm}^{-2}$ | $2.6e+03 \text{ cm}^{-2}$ | $1.3e+12 \text{ cm}^{-2}$ | $1.1e+10 \text{ cm}^{-2}$ | $2.3e+09 \text{ cm}^{-2}$ |
| f_{vol} | 0.05 | 0.2 | 0.4 | 0.05 | 0.2 | 0.4 |
| $f_{\text{ic}} = 0.1$ | $1.4e+01$ | $3.6e+00$ | $2.0e+00$ | $3.2e+02$ | $1.7e+01$ | $4.7e+00$ |
| $f_{\text{ic}} = 0.3$ | $7.3e+00$ | $2.4e+00$ | $1.6e+00$ | $1.1e+02$ | $8.6e+00$ | $3.1e+00$ |
| $f_{\text{ic}} = 0.5$ | $3.7e+00$ | $1.7e+00$ | $1.4e+00$ | $3.6e+01$ | $2.1e+00$ | $5.3e+00$ |
| Smooth | | $2.6e+09 \text{ cm}^{-2}$ | $3.0e+02 \text{ cm}^{-2}$ | $9.3e+09 \text{ cm}^{-2}$ | $2.2e+09 \text{ cm}^{-2}$ | $3.4e+08 \text{ cm}^{-2}$ |
| f_{vol} | 0.05 | 0.2 | 0.4 | 0.05 | 0.2 | 0.4 |
| $f_{\text{ic}} = 0.1$ | $4.3e+00$ | $1.9e+00$ | $1.4e+00$ | $1.3e+02$ | $7.9e+00$ | $4.7e+00$ |
| $f_{\text{ic}} = 0.3$ | $2.9e+00$ | $1.6e+00$ | $1.3e+00$ | $6.0e+01$ | $3.1e+00$ | $1.8e+00$ |
| $f_{\text{ic}} = 0.5$ | $2.0e+00$ | $1.4e+00$ | $1.3e+00$ | $2.4e+01$ | $2.1e+00$ | $1.5e+00$ |

Notes. Corresponding abundance profiles are shown in Fig. F.4. We note that the models with $f_{\text{vol}} = 0.4$ have the same porosity length $h_* = 2.5 \times 10^{13} \text{ cm}$ as the one-component models with $f_{\text{vol}} = 0.2$, $I_* = 5 \times 10^{12} \text{ cm}$ and $f_{\text{vol}} = 0.4$, $I_* = 1 \times 10^{13} \text{ cm}$. Differences larger than one order of magnitude are in boldface.